NASA CR-165395

DEVELOPMENT OF IMPROVED HIGH TEMPERATURE COATINGS FOR IN-792 + Hf

D.D. Profant
S.K. Naik

AVCO LYCOMING DIVISION
Material Laboratory
550 South Main Street
Stratford, Connecticut 06497

CONTRACT NAS3-22371
FINAL REPORT
JUNE 1981

Prepared For

U.S. ARMY AVIATION RESEARCH AND DEVELOPMENT COMMAND
USARTL Propulsion Laboratory

and

NATIONAL AERONAUTICS AND SPACE ADMINISTRATION
NASA Lewis Research Center
Cleveland, Ohio 44135

1. Report No.	2. Government Accession No.	3. Recipient's Catalog No.
NASA CR-165395		

4. Title and Subtitle	5. Report Date
DEVELOPMENT OF IMPROVED HIGH TEMPERATURE COATINGS FOR IN-792 + Hf	JUNE 1981
	6. Performing Organization Code
7. Author(s)	8. Performing Organization Report No.
D. D. PROFANT and S. K. NAIK	
	10. Work Unit No.
9. Performing Organization Name and Address: AVCO LYCOMING DIVISION, MATERIAL LABORATORY, 550 So. MAIN STREET, STRATFORD, CT. 06497	11. Contract or Grant No. NAS3-22371
12. Sponsoring Agency Name and Address: U. S. Army Aviation Research and Development Command, USARTL Propulsion Laboratory, Cleveland, OH 44135	13. Type of Report and Period Covered: CONTRACTOR REPORT
	14. Sponsoring Agency Code: 1L162209AH76

15. Supplementary Notes: FINAL REPORT
Project Manager: Dr. Stanley R. Levine, Head, Coatings Section, NASA-Lewis Research Center, Cleveland, Ohio 44135

16. Abstract

The objective of the program was to advance the technology of high temperature coatings for IN-792 + Hf cast integral turbine nozzles by indicating most promising directions for developing coatings with improved thermal fatigue resistance without sacrificing oxidation/corrosion protection. The program evaluated 10 coating systems which comprised one (1) baseline plasma spray coating (12% Al-NiCoCrAlY), three (3) aluminide coatings including the baseline aluminide (701), two (2) CoNiCrAlY (6% Al) + aluminide systems and four (4) NiCoCrY + aluminide coating systems. The two-step coating processes were investigated since it offered the advantage of "tailoring" the composition as well as properly coating all surfaces (including the internal cooling passages) of an integral or segmented nozzle. Cyclic burner rig thermal fatigue and oxidation/corrosion tests were used to evaluate the candidate coating systems. The plasma sprayed 12% Al-NiCoCrAlY was rated the best coating in thermal fatigue resistance and outperformed all coatings by a factor between 1.4 to 2.5 in cycles to crack initiation. However, this coating is not applicable to integral or segmented nozzles due to the line of sight limitation of the plasma spray process. The 6% Al-CoNiCrAlY + Mod. 701 aluminide (32 w/o Al) was rated the best coating in oxidation/corrosion resistance. Its coating life was greater than the NiCoCrAlY (12% Al), 701 aluminide (40 w/o Al) and the NiCoCrY + RT21 (25 w/o Al) by a factor of 1.3, 1.5 and 2.0 respectively. This coating, along with the 701 aluminides, was in the group of coatings rated the second best in thermal fatigue resistance.

17. Key Words (Suggested by Author(s))	18. Distribution Statement
Plasma sprayed MCrAlY, MCrY coatings Aluminide coatings Two step coatings (Plasma Spray + Aluminide) Thermal fatigue resistance Oxidation/Corrosion resistance	Unclassified-Unlimited

19. Security Classif. (of this report)	20. Security Classif. (of this page)	21. No. of Pages	22. Price*
Unclassified	Unclassified	85	

* For sale by the National Technical Information Service, Springfield, Virginia 22161

N82-14333#

FOREWORD

This final report covers the activity performed under a six month NASA-Lewis Research Center contract NAS3-22371. Dr. Stanley Levine of the NASA-Lewis Research Center served as Project Manager for this Program. The work was funded by the Propulsion Laboratory, U.S. Army Research and Technology Laboratories, U.S. Army Aviation Research and Development Command.

This report was prepared by the Avco Lycoming Division, Materials Laboratories, Stratford, Connecticut with Mr. D.D. Profant as the project manager and Dr. S.K. Naik as the principal investigator.

The authors wish to acknowledge the contribution provided by the following individuals:

P. Follo	Electron microprobe and X-ray analysis.
J. Podlisny	Burner rig testing.
T. Beers	Metallographic assistance.

TABLE OF CONTENTS

LIST OF TABLES

LIST OF ILLUSTRATIONS

LIST OF ILLUSTRATIONS (CONT'D)

LIST OF ILLUSTRATIONS (CONT'D)

LIST OF ILLUSTRATIONS (CONT'D)

LIST OF ILLUSTRATIONS (CONT'D)

1.0 SUMMARY

Recent requirements to uprate the performance of Avco Lycoming T55-L11 turbine engines led to severe cyclic thermal exposures which produced cracking on the vane leading edges of the Lycoming 701 pack aluminide coated C101 (IN-792 + 1% Hf) integral nozzle.

The objective of the program was to advance the technology of high temperature coatings for cast integral nozzles. Coating concepts that would retain the oxidation and corrosion protection of the 701 coating, but delay the onset and reduce the number of vane leading edge cracks were investigated.

The line of sight restrictions of the common overlay deposition processes (electron beam, plasma spray) prevent proper application of a "ductile" MCrAlY type composition except on the leading edge area of an integral or segmented nozzle. This program, therefore, investigated the approach of developing a two-step coating process whereby a MCrY or MCrAlY (low aluminum) composition was plasma sprayed and overcoated by a candidate pack aluminide process. This processing technique offered the advantage of "tailoring" the composition as well as properly coating all surfaces (including the internal cooling passages) of the integral nozzle.

The program evaluated 10 coating systems which comprised one (1) baseline plasma spray coating (12% Al-NiCoCrAlY), three (3) aluminide coatings including the baseline aluminide (701), two (2) CoNiCrAlY (6% Al) + aluminide systems and four (4) NiCoCrY + aluminide coating systems.

The thermal fatigue testing of all coating systems was conducted in a natural gas fuel fired rig utilizing a four minute cycle (1038°C/2 min./water quench). Oxidation/corrosion tests were conducted on six selected systems in a burner rig using JP-5 (.2% S) fuel and utilizing a two temperature-set point, six minute cycle (900°C, 2 min./1065°C, 2 min./water cool).

The plasma sprayed 12% Al-NiCoCrAlY was rated the best coating in thermal fatigue resistance and outperformed all other coatings by a factor between 1.4 to 2.5 in cycles to crack initiation. However, this coating is not applicable to integral or segmented nozzles for reasons mentioned above. The 6% Al-CoNiCrAlY + Mod. 701 aluminide (32 w/o Al) was rated the best coating in oxidation/corrosion resistance. Its coating life was greater than the NiCoCrAlY (12% Al), 701 aluminide (40 w/o Al) and the NiCoCrY + RT21 (25 w/o Al) by a factor of 1.3, 1.5 and 2.0 respectively. This coating, along with the 701 aluminides, was in the group of coatings rated the second best in thermal fatigue resistance.

2.0 INTRODUCTION

2.1 Background

For several years, Avco Lycoming T55-L11 turbine engines have successfully operated with cast integral nozzles of IN-713C alloy coated with Lycoming 701 pack aluminide. The use of the integral nozzle has resulted in significant cost savings over the individual vane concept and the Lycoming 701 aluminide coating has imparted excellent oxidation/corrosion resistance. Recent requirements to uprate performance led to the introduction of 701 coated C101 (IN-792 + 1% Hf). Even though IN-792 + 1% Hf has significantly improved strength and oxidation/corrosion resistance over IN-713C, the more severe cyclic thermal exposure associated with the T55-L712 engine causes cracking on vane leading edges. While design changes have helped to mitigate the effects of the thermal cycling, it is apparent that a more ductile coating system is required to reduce the susceptibility of the nozzle to thermal-fatigue cracking.

It has been established that appropriately balanced compositions of MCrAlY (refs. 1, 2 and 3) overlay coatings provide both good thermal fatigue resistance and effective high temperature oxidation/corrosion protection. However, an inherent disadvantage of the most common overlay coating deposition processes (electron beam, plasma spray, sputtering) is that the technique limits coverage to line of sight surfaces. This restriction prevents proper coverage except on the leading edge area of an integral or segmented nozzle. For these components, it would be most logical from a processing standpoint if a two-step coating system could be applied wherein an MCrY or MCrAlY (low aluminum) overlay was plasma sprayed onto the leading edges and the remaining surfaces (including the internal cooling passages) were subsequently aluminized to a controlled surface aluminum content. This concept is derived from

earlier NASA research (4, 5). This processing technique offers the advantage of "tailoring" the composition of the coating for specific applications so as to obtain a balance between ductility and oxidation/corrosion protection.

The objective of this program was to advance the technology for high temperature coatings applicable to a cast integral IN-792 + 1% Hf alloy nozzle that would retain the oxidation and corrosion protection of Lycoming 701 pack aluminide, but delay the onset and reduce the number of thermal fatigue cracks.

2.2 Approach

Two primary approaches were pursued to develop a more ductile, improved thermal-fatigue resistant coating. One approach was to identify a lower aluminum content pack aluminide coating and the second was to identify a two-step coating by applying a plasma sprayed coating followed by an aluminide overcoat. In order to evaluate the second approach, test specimens were plasma sprayed with MCrY or MCrAlY (low aluminum) powder compositions and overcoated by several pack aluminide processes chosen to result in coatings with various aluminum contents.

A grid showing the 10 coating systems evaluated along with the plasma spray powder alloy compositions is shown in Figure 1. The program flow chart is shown in Figure 2. The Lycoming 701 pack aluminide coating and the 12% Al content NiCoCrAlY plasma sprayed coating, which exhibited effective thermal fatigue resistant properties in previous NASA-IITRI tests, were included in the ten coated systems as reference basis for aluminide and plasma coated systems. The remaining coating systems included modifications of the pack aluminide with lower aluminum content or combinations of the pack aluminides as overcoats to the plasma sprayed MCrY or

MCrAlY coatings. Three (3) different MCrY powder compositions and a 6% Al content CoNiCrAlY composition were evaluated as plasma applied undercoats.

The thermal fatigue testing of all coating systems was conducted in a natural gas fuel fired rig. A JP-5 fuel fired burner rig facility was utilized to conduct the oxidation/sulfidation tests on the six systems marked with an asterisk in Figure 1.

PLASMA COATINGS (UNDERCOAT)	ALUMINIDE COATINGS (OVERCOAT)			
	None	701	MOD. 701	RT21
None		#1 *	#2	#3
M3958+ (Ni-23Co-18Cr-12Al-.6Y)	#4*			
M3959+ (Co-29Ni-26Cr-6Al-.6Y)		#5	#6*	
M39AA+ (Ni-5Co-35Cr-.6Y)				#7*
M39AB+ (Ni-15Co-35Cr-.6Y)				#8*
M39AC+ (Ni-15Co-20Cr-.6Y)			#10	#9*

+ Designates Avco Lycoming Specification Number for Powder Alloy.

* Coating Systems Selected for Oxidation/Corrosion Tests. All Coatings Evaluated By Thermal Fatigue.

Figure 1: Experimental Box Grid of The Candidate Coating Systems.

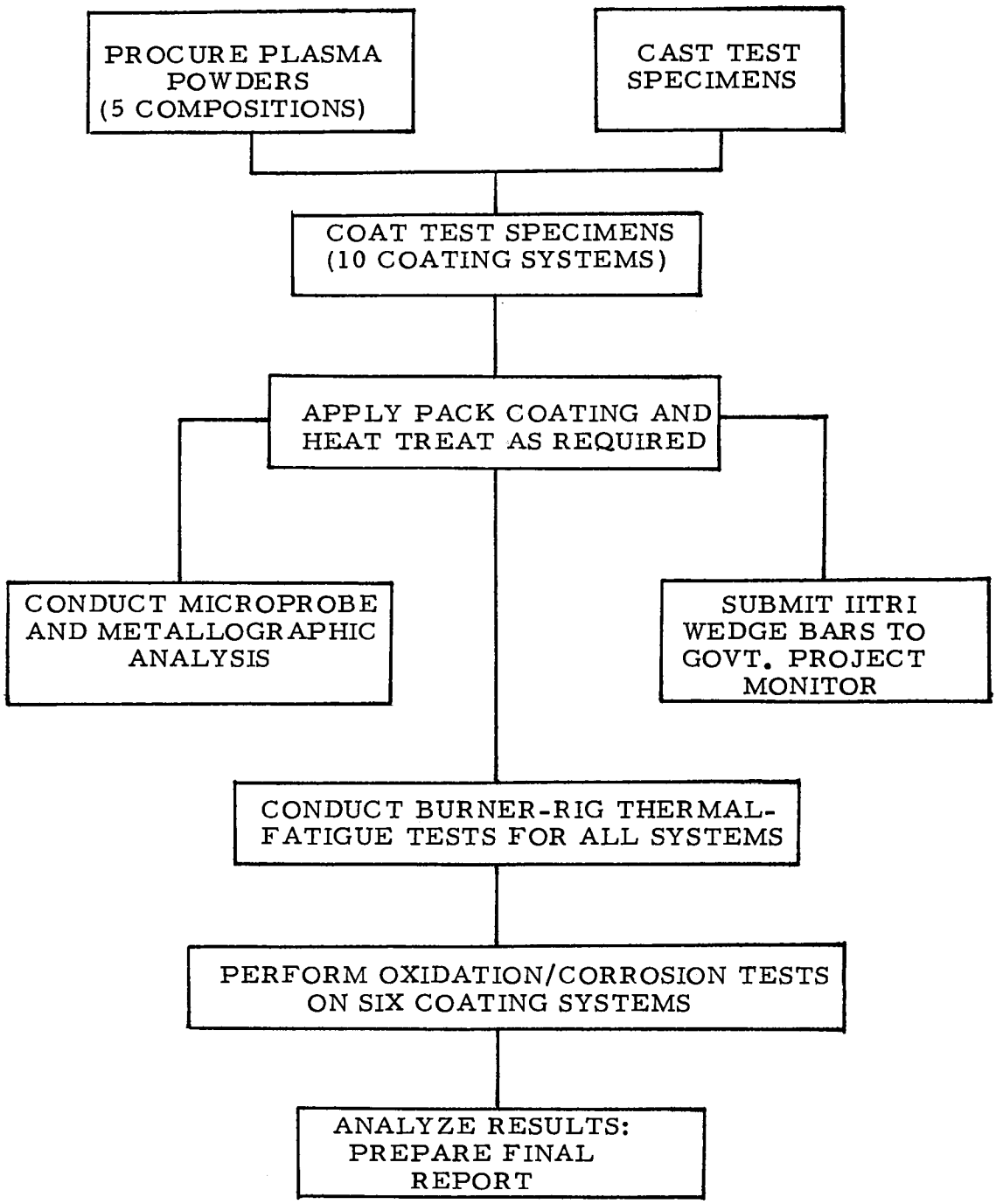

Figure 2. Program Flow Chart

3.0 EXPERIMENTAL PROCEDURE

3.1 Specimen Fabrication

The substrate material used in this program was a cast C101 alloy which was vacuum melted by Cannon-Muskegon. The nominal composition of the alloy is contained in Table 1. C101 is a Lycoming modification of IN-792 with Hf additions and is the current bill of material for the hot section components of Lycoming's higher performance engines.

All specimens were cast by Jetshapes in accordance with standard Lycoming procedure for turbine blades. A photograph of the oxidation/corrosion airfoil test specimen, Lycoming modified thermal fatigue double wedge bar and the NASA/IITRI double wedge specimen is shown in Figure 3. Figure 4 shows the dimensions of each specimen.

The cast test specimens obtained from Jetshapes were examined for surface flaws and internal shrinkage/porosity by fluorescent penetrant and radiographic methods. Minor internal shrinkage was detected in the critical areas of the cast test specimens. The specimens were therefore hot isostatically pressed at 1185°C/4 Hrs at 172 MPa to eliminate the internal flaws. Grain size characterization was completed on several randomly selected thermal fatigue wedge specimens. The critical areas of the acceptable cast test specimens conformed to the following:

1. Uniform equiaxed grains approximately 1.58 mm in diameter.
2. All test specimens were sound and free from surface flaws or internal defects.
3. The surfaces of the test specimens were smooth and clean.

3.2 Selection of Candidate Coating Systems

The rationale for the selection of the 10 coated systems shown in the experimental grid of Figure 1 is described below.

System 1: Standard Lycoming pack 701 aluminide which was included

TABLE 1: Nominal Composition of C101 Alloy.

Element	Wt. %
Cr	12.6
Co	9.0
Mo	1.95
W	3.95
Ta	3.95
Ti	4.1
Al	3.3
Hf	1.0
C	0.16
B	0.01
Zr	0.11
Ni	Balance

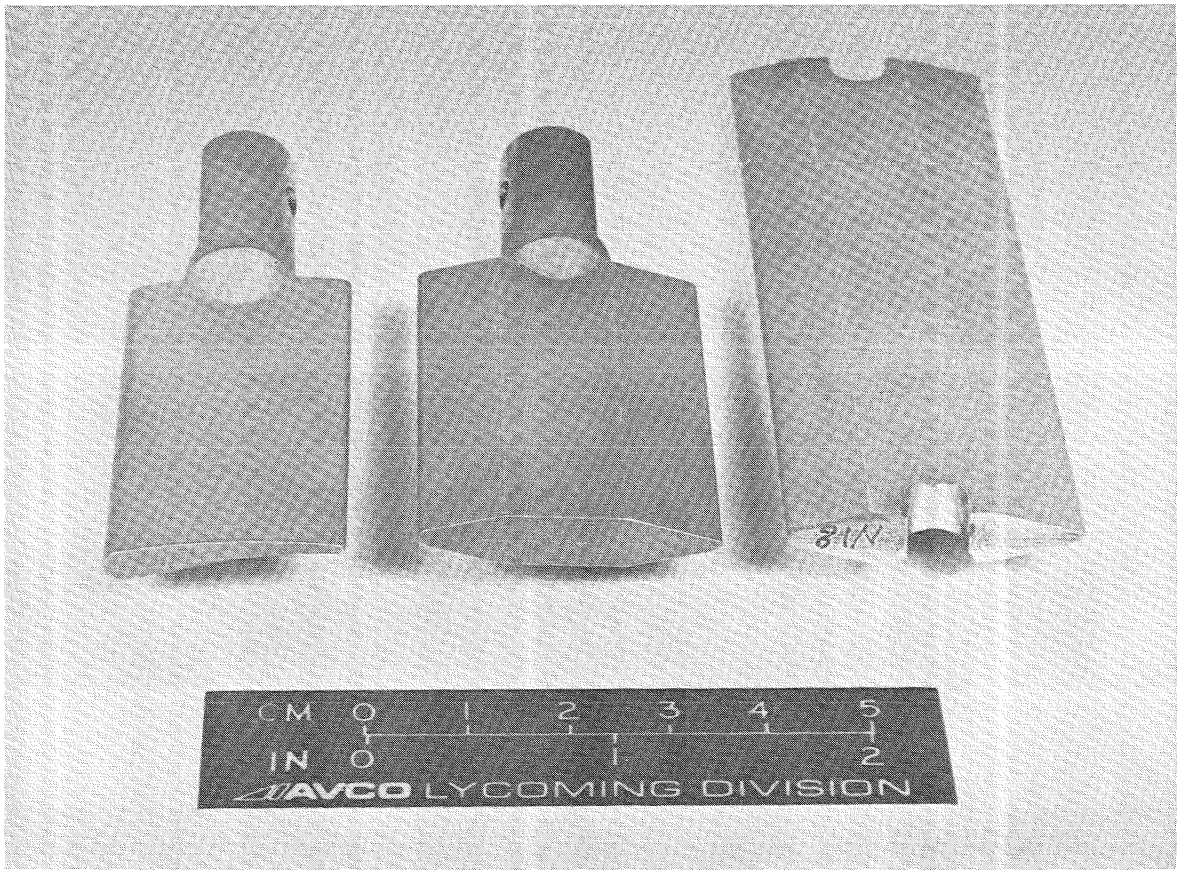

Figure 3 Cast Test Specimens L to R: Oxidation/Corrosion Airfoil Test Paddle, Lycoming Thermal Fatigue Wedge Bar, NASA/IITRI Thermal Fatigue Wedge Bar.

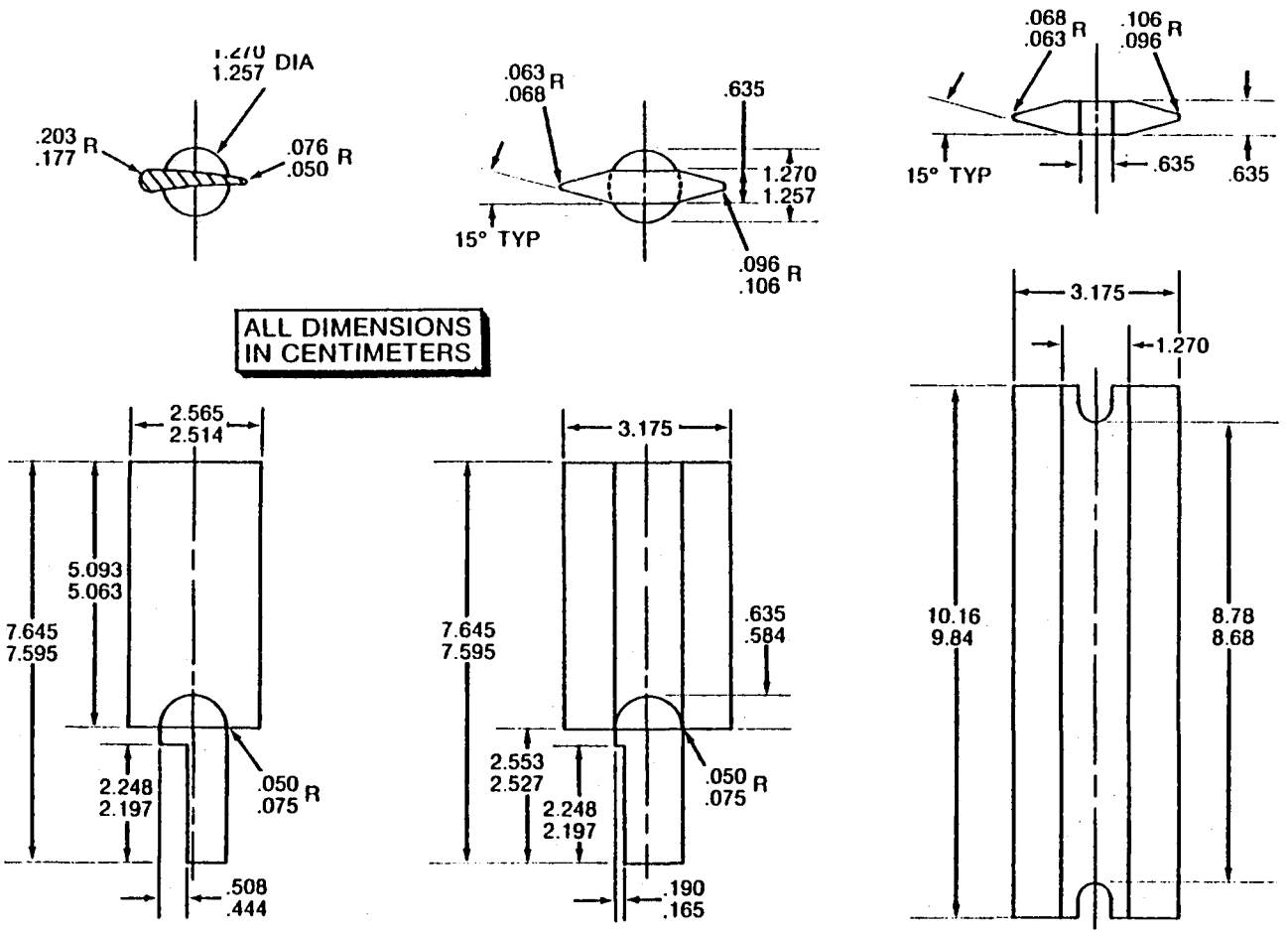

Figure 4 Dimensions of Test Specimens L to R: Oxidation/Corrosion Test Paddle, Lycoming Thermal Fatigue Wedge Bar, NASA/ IITRI Thermal Fatigue Wedge Bar.

as a reference coating.

System 2: Modified 701 which is a reduced thickness coating plus a vacuum diffusion cycle. This system is intended to improve ductility by reducing the surface aluminum content through a subsequent diffusion heat treatment (1065°C/4 Hrs).

System 3: RT-21 pack aluminide applied by a vendor, followed by a diffusion heat treatment (1065°C/4 Hrs) in an inert environment to produce an aluminide coating with 25-30 w/o surface aluminum.

The above three aluminide coating systems are simple pack processes which incorporated no plasma sprayed coatings. These systems were included since they represented a minimum amount of development effort and a low cost approach. The remaining seven (7) systems incorporated plasma sprayed coatings. All plasma sprayed coatings were deposited in a low pressure chamber to a thickness of 50 to 100 μm and a minimum density of 98%, and were glass bead peened in order to improve density.

System 4: Plasma sprayed Ni-23Co-18Cr-12Al-.6Y. This system was included as a reference since previous NASA/IITRI tests demonstrated that this composition had excellent thermal-fatigue resistance.

System 5: Plasma sprayed Co-29Ni-26Cr-6Al-.6Y with a standard 701 pack overcoat.

System 6: Plasma sprayed Co-29Ni-26Cr-Al-.6Y with a modified 701 pack overcoat.

The above two systems resulted in a varied surface aluminum content over the 6% Al content CoNiCrAlY undercoat, with #5 having the higher surface aluminum content and system #6 being lower. The thermal-fatigue test data on these systems would provide one comparison for assessing the effect of surface aluminum content on fatigue life.

The remaining systems involved NiCoCrY based compositions and eval-

uated the effects of Cr and Co variations in the plasma sprayed systems with aluminide overcoats.

System 7: Plasma sprayed Ni-5Co-35Cr-.6Y with an aluminide pack overcoat as described in system #3.

System 8: Plasma sprayed Ni-15Co-35Cr-.6Y with an aluminide pack overcoat as described in system #3.

System 9: Plasma sprayed Ni-15Co-20Cr-.6Y with an aluminide pack overcoat as described in system #3.

System 10: Plasma sprayed Ni-15Co-20Cr-.6Y with a modified 701 pack aluminide overcoat.

While it was recognized that the above systems did not represent a complete matrix of variables, it was anticipated that evaluation of the ten systems would result in a suitable coating process or at the very least point to an approach that ultimately could result in a satisfactory coating process.

3.3 Coating Fabrication

A total of five (5) compositions of plasma spray powders were procured and evaluated in the program. All powders except M3958 were procured from Alloy Metals Inc. according to applicable Lycoming specifications. M3958 powder alloy was procured through NASA. The powders complied with the following nominal composition:

a) M3958: Ni-23Co-18Cr-12Al-.6Y

b) M3959: Co-29Ni-26Cr-6Al-.6Y

c) M39AA: Ni-5Co-35Cr-.6Y

d) M39AB: Ni-15Co-35Cr-.6Y

e) M39AC: Ni-15Co-20Cr-.6Y.

A box grid of the candidate coating systems is shown in Figure 1. The coating of the test specimens for systems 1 (701) and 2 (Mod. 701) were performed in-house. All other coating systems were applied by Chromalloy Corporation. Brief descriptions of the aluminide and the plasma

spray coating processes are given below.

o Aluminide Coatings

The Lycoming 701 aluminide is a pack cementation coating with a typical pack weight percent composition of; 67% (55Cr-45Al alloy powder) + 33% Al_2O_3 and the required activator content. The coating is accomplished in a vacuum furnace with the pack held at 1038°C for a period of time ranging from 3 to 5 hours sufficient to give an acceptable Lycoming specification coating thickness between 38 μm - 100 μm. The modified 701 coating process essentially consists of depositing a thinner coating (38 μm - 70 μm) and subjecting the coated parts to a subsequent diffusion heat treatment at 1065°C for 4 hours in argon/air atmosphere. RT21 is a proprietary Chromalloy pack coating designed to give a 50 μm - 75 μm thick coating with 25 - 30% Al at the coating surface.

o Plasma Spray Coatings

The plasma spraying was conducted in a low pressure chamber to develop a thickness between 76μm-127μm and an acceptable density of 98%. All plasma spray coated specimens were glass bead peened at 6-7N intensity and diffusion heat treated at 1065°C for 4 hours.

For each of the ten (10) coating systems, four (4) Lycoming thermal-fatigue bars, three (3) standard IITRI wedge bars and three (3) oxidation/corrosion test paddles were coated. One of the four Lycoming fatigue bars was used for metallographic and microprobe analysis, while the remaining were used for thermal fatigue testing. All coated IITRI wedge bars were forwarded to the NASA Project Manager for testing in a fluidized bed facility.

3.4 Coating Evaluation

Burner-rig test facilities were utilized to perform the thermal fatigue and oxidation/corrosion testing. A photograph of the JP-5 fuel fired test rig used for oxidation/corrosion is shown in Figure 5 and schematically

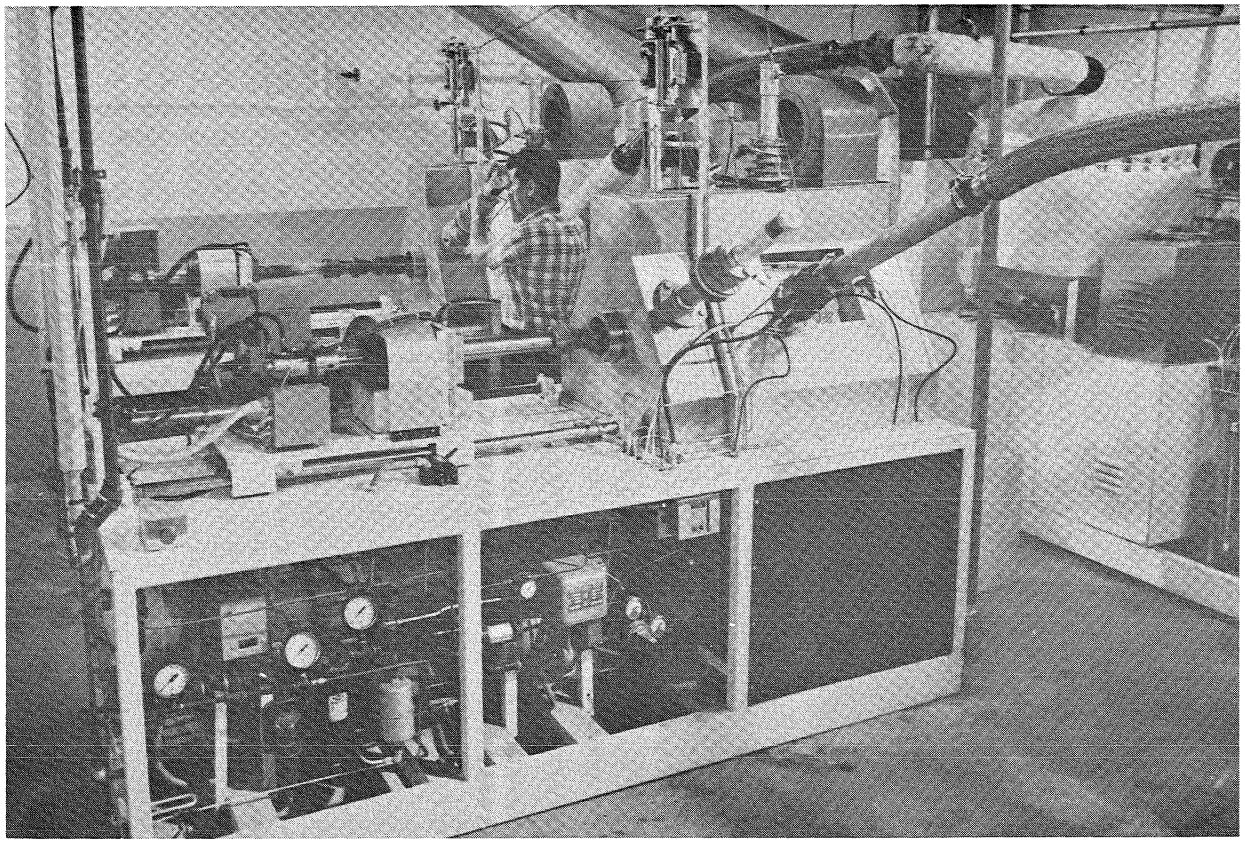

Figure 5 Fuel Fired Burner Test Rig.

in Figure 6. The thermal fatigue testing was conducted on a natural gas fired fuel rig. An effective means of testing for thermal-fatigue resistance is to expose a double wedge shaped specimen (see Figure 3) to rapid thermal cycling. Due to differences in thermal mass, the thinner wedge section will expand and contract upon heating and cooling at a faster rate than the thicker section. By continually cycling the specimen in and out of a high temperature zone, such as a fluidized bed or a combustion flame, the specimen undergoes a thermally induced fatigue loading cycle. Because of the limited duration of the program, all rig tests were conducted under relatively accelerated conditions. The frequency of the heating and cooling cycles, the test temperatures, the thermal shock (water quench) methods, and the rate of ingestion of the contaminating species were the main test variables used to control severity. The test facilities and test evaluation procedures are discussed below.

3.4.1 Thermal Fatigue Gas Fired Rig Facility

The gas fired rig, which is similar in appearance to the fuel fired rig, is a self contained unit consisting of the gas, combustion air, pneumatic, and water quench control systems. The gas and combustion air systems are controlled through an electrical system which includes safety circuits for proper ignition of the gas burners. The burners are capable of providing 73.2KW of heat at the maximum setting. The control system utilizes timers which control the initiation and duration of the heating and cooling cycles as well as the air and water solenoid valves. The heating and cooling cycles can be preset over a wide range. The specimen holder is a water cooled specimen shaft and is mounted on bearings which permits movement of the specimen shaft assembly into and out of the furnace. A coupling mounted on the outside of the shaft rotates the specimens to a speed of 1750 rpm. A radiation pyrometer is used to sense and control the metal temperature. When the heating cycle is completed, the specimens

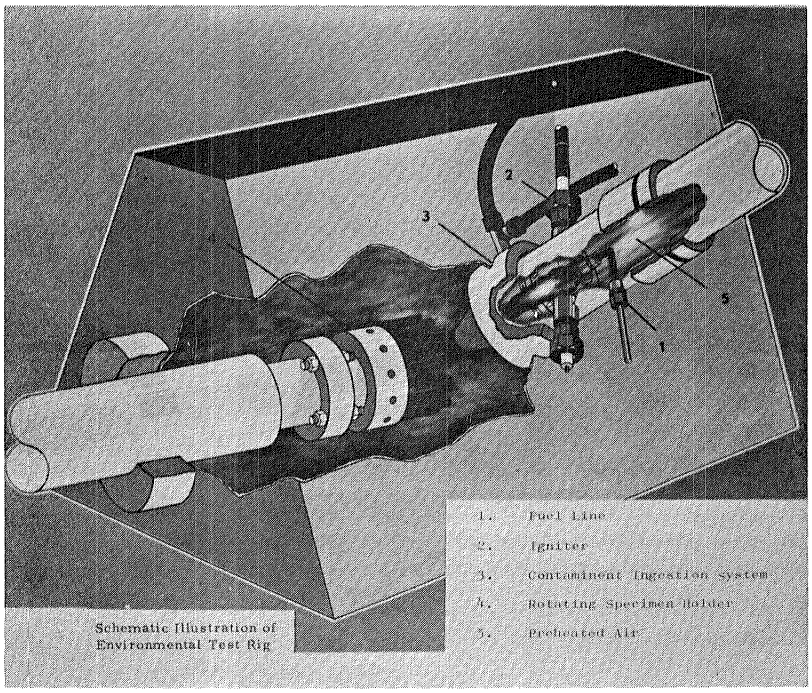

Figure 6 Schematic Illustration of Burner Rig.

are retracted into a cooling chamber, where the cooling water jet is activated. The cycle automatically restarts at the end of the cooling cycle.

3.4.2 Thermal Fatigue Test Procedure

All candidate coating systems were screened for thermal fatigue cracking performance utilizing a four minute cycle. The test cycle consisted of holding the specimens at 1038°C for 2 minutes followed by a water quench (see Figure 7). The wedge specimens were placed with the small radius towards the burner flame as shown in Figure 8. The specimens were examined at regular cycle intervals to determine the initiation and the rate of crack propagation. Typically, the specimen was removed from test when a crack was observed on the small radius wedge surface and extended beyond on both faces. The ranking of the various coatings were based on the combination of the following factors:

(1) Cycles to initial crack appearance.

(2) Total number of cracks observed at the end of 1050 cycles of test.

(3) Metallurgical examination of the nature and extent of the fatigue cracks. In addition, one coated specimen within each system was stripped after test and the crack lengths were compared to the lengths recorded before stripping.

3.4.3 Oxidation/Corrosion Fuel Fired Rig Facility

The liquid fuel test rig is a self contained facility with its own air compressor, air preheater, test chamber and fuel system. High velocity gases of approximately 215 m/s are impinged against the airfoil test specimens, as shown schematically in Figure 6, to raise them to the desired temperature. A converging nozzle is used to direct and concentrate the flame on the specimens. Synthetic sea water is injected into the gas stream just below the skirt of the combination liner. The combustor burned JP-5 fuel for this test; the pressure in the test chamber is essentially atmospheric.

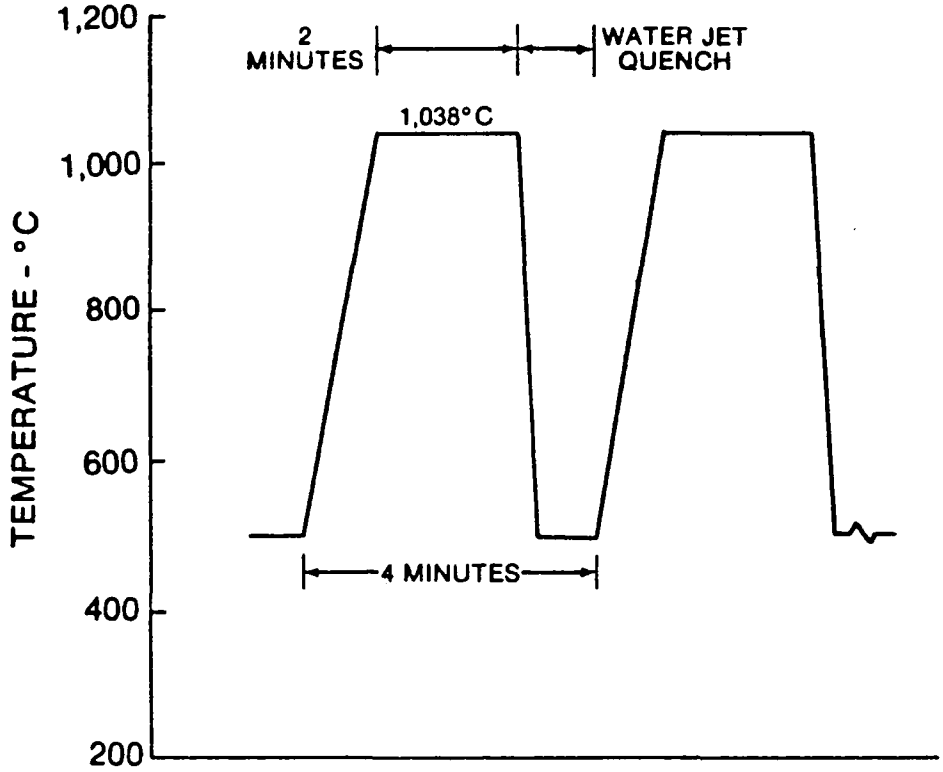

Figure 7 Schematic of Thermal Fatigue Test Cycle.
Heat Cycle: 1038°C/2 minutes; Fuel: Gas Fired.
Water Jet Quench Rate: 10 gm/sec and 18 gm/sec.

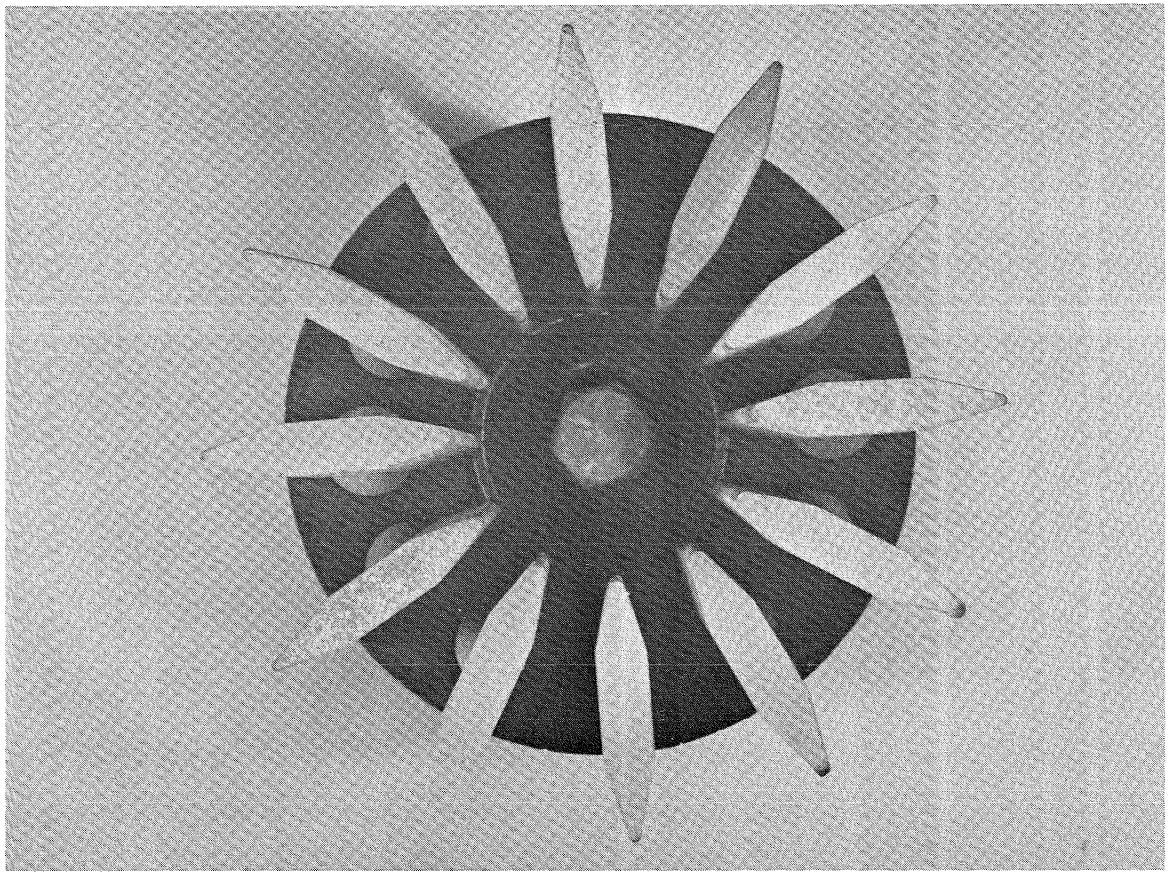

Figure 8 Top View of Specimen Holder Showing Arrangement of Wedge Bars with Small Radius on the Outside Diameter.

The air to fuel ratio ranges from about 28:1 - 33:1 depending on the test temperature. Air flow is maintained constant at .0378 kg/sec at 285°C while the fuel flow is controlled by means of a radiation pyrometer which senses the metal temperatures. The specimen holder is rotated in order to expose all specimens uniformly. Heating and cooling cycles are accomplished by alternately translating the specimen holder between the furnace heating and cooling chambers. Thermal cooling can be imposed by air, water mist, and/or water jet.

3.4.4 Oxidation/Corrosion Resistance Test Procedure

The tests were conducted on the six coating systems as noted in Figure 1 using the Lycoming airfoil paddle specimens. A two temperature-set point, six minute cycle (900°C, 2 min/1065°C, 2 min./water cool) was used for the testing of the coated airfoil paddles as illustrated in Figure 9. The salt/air ratio was maintained at 6ppm and 0.2% sulfur was added to the JP-5 fuel. Twelve airfoil test specimens (see Figure 10) were placed in the specimen holder with the leading edge (large radius) facing outward. The test specimen were weighed and visually inspected at 20 hour intervals.

Coating failure was arbitrarily established as occuring when 0.1 cm^2 of the base metal was exposed. The weight gain/loss data were tabulated. The ranking of the coating systems was based on the coating life expressed in minutes/micron of coating thickness. One test specimen of each coating was metallurgically evaluated after test completion. The change of coating microstructure and chemical composition which occurred during test was ascertained by XRD & EMP in order to define the principle mode of coating failure and/or degradation.

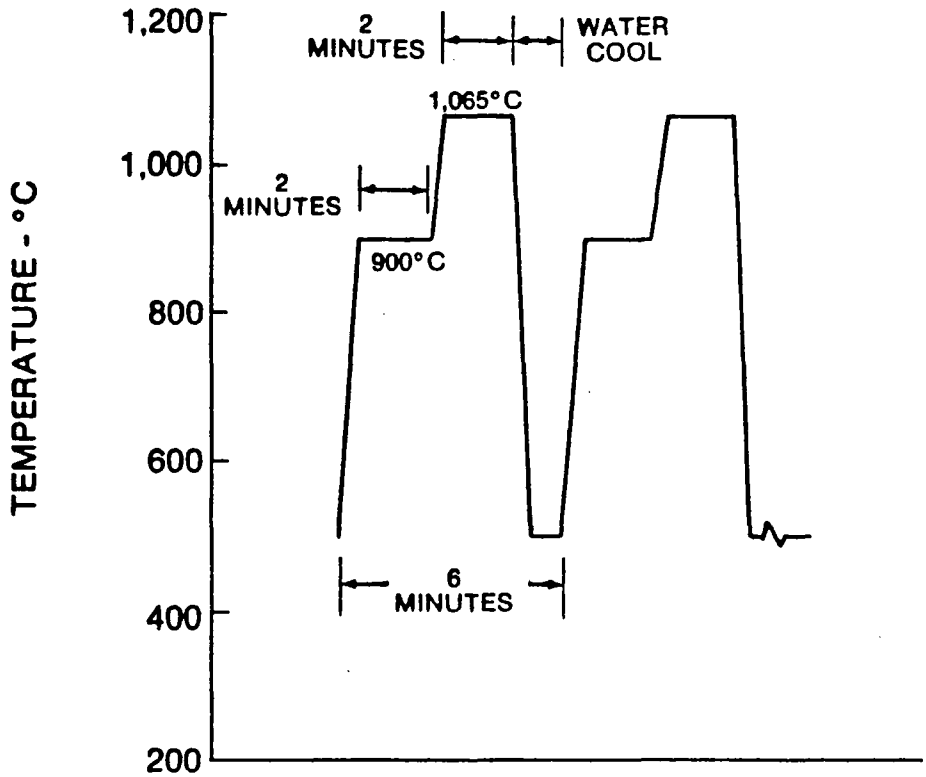

Figure 9 Schematic of Oxidation/Corrosion Test Cycle.
Heat Cycle: 900° C, 2 min./1065° C, 2 minutes.
Fuel: JP-5 (0.2 wt.% S); Salt/Air Ratio: 6 ppm.

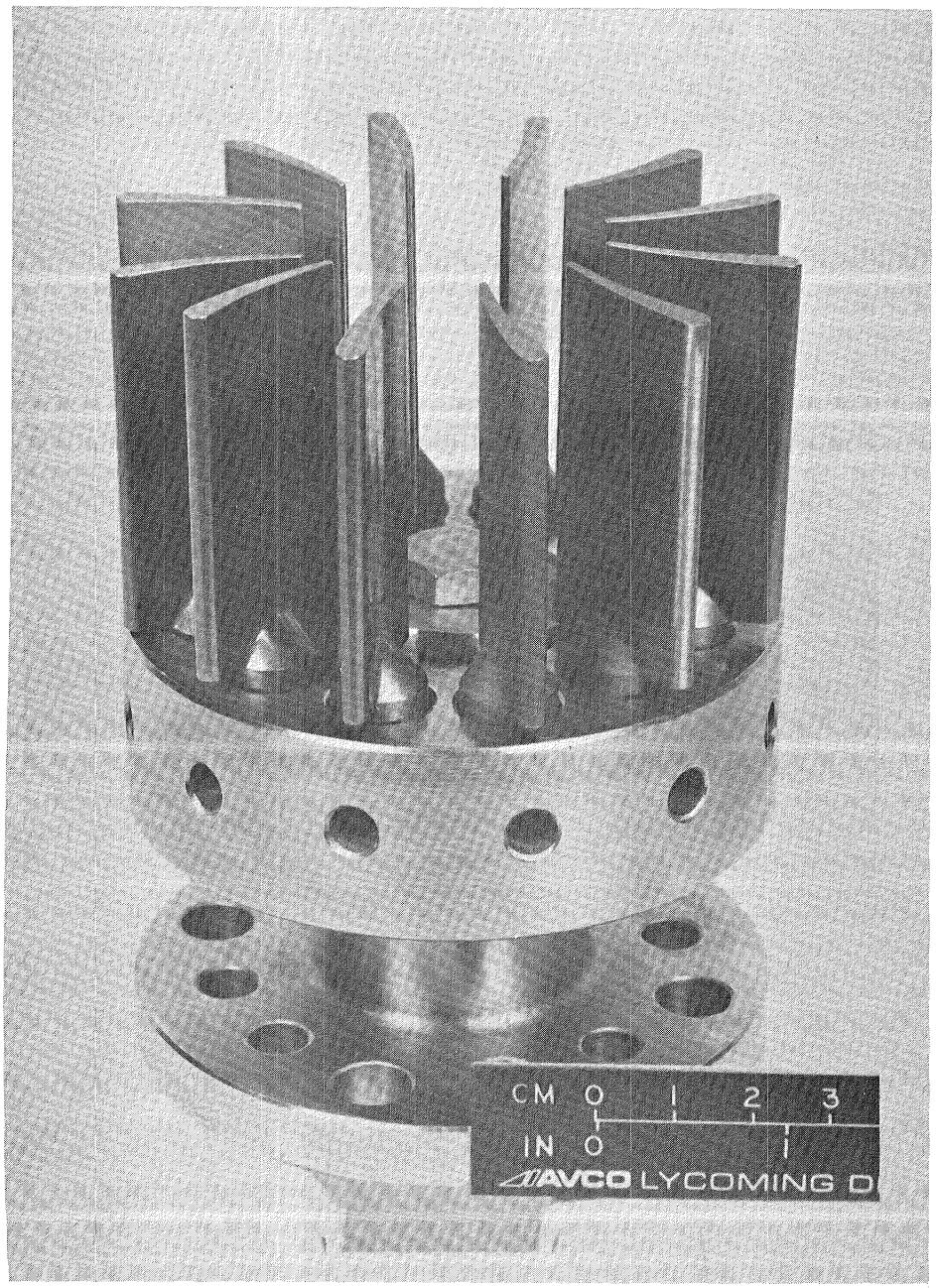

Figure 10 Specimen Holder showing Arrangement of Oxidation/Corrosion Airfoil Test Specimens with Leading Edge on the Outside Diameter.

4.0 RESULTS AND DISCUSSION

4.1 Coating Systems

The pretest microstructure and the microprobe profile of the 10 coating systems are shown in Figures 11-20. A summary of the metallurgical evaluation of the coating systems is given in Table 2. All further discussion of the various coating systems are referenced to the coating system number and/or coating type as noted in Table 2. Table 2 also provides descriptions of the coatings, the original coating thickness, and a microprobe analysis summary of the aluminum concentration (w/o) of each coating.

The plasma spray + aluminide coating systems (System Nos. 5-10, Figures 15-20) exhibit a high aluminum content outer zone. The concentration (w/o) of aluminum in the outer zone is noted in Table 2. The aluminum concentration was judged to be uniform throughout the coating thickness for the pack aluminide systems (701, Mod. 701, RT21) and the baseline 12% Al-NiCoCrAlY (M3958) plasma sprayed system (Figures 11-14). The plasma sprayed + aluminide coating systems exhibited a minor amount of porosity/inclusions within the plasma sprayed portion as well as at the coating/substrate interface. A discussion of the candidate coating systems is given below.

a) Pack Aluminide Coatings

The 701 pack aluminide had a coating thickness of 95μm with a uniformly dense microstructure. The coating exhibited a structure with about 40 wt.% aluminum (Figure 11). The Modified 701 coating was 63.5μm thick with 32 wt % aluminum and evidence of minor porosity within the diffusion zone of the coating (Figure 12). The RT21 pack aluminide coating deposited by Chromalloy was 51μm thick and had a β (NiAl) structure with about 25 wt.% aluminum. Minute amounts of inclusions were noted at random locations along the diffusion zone

TABLE 2: Coating Thickness and Microprobe Analysis Summary of Coating Systems.

COATING SYSTEM			Total Coating Thickness, Microns	Aluminum Rich Zone Thickness, Microns	Wt % Al in Aluminum Rich Zone
System No.	Coating Type	Coating Description			
1	701	Pack Aluminide	95	95	40
2	MOD. 701	Lower Activity Pack Aluminide + Diffusion	63.5	63.5	32
3	RT21	Pack Aluminide (Vendor)	51	51	25
4	M3958	(Ni-23Co-18Cr-12Al-.6Y)	76	76	12
5	M3959+701	(Co-29Ni-26Cr-6Al-.6Y)	140	76	38
6	M3959+MOD. 701	(Co-29Ni-26Cr-6Al-.6Y) + MOD. 701	89	38	32
7	M39AA+RT21	(Ni-5Co-35Cr-.6Y) + RT21	70	26	24
8	M39AB+RT21	(Ni-15Co-35Cr-.6Y) + RT21	82.5	26	26
9	M39AC+RT21	(Ni-15Co-20Cr-.6Y) + RT21	57	19	15
10	M39AC+MOD. 701	(NI-15Co-20Cr-.6Y) + MOD. 701	76	51	34

Note: All MCrY or MCrAlY compositions were plasma sprayed.

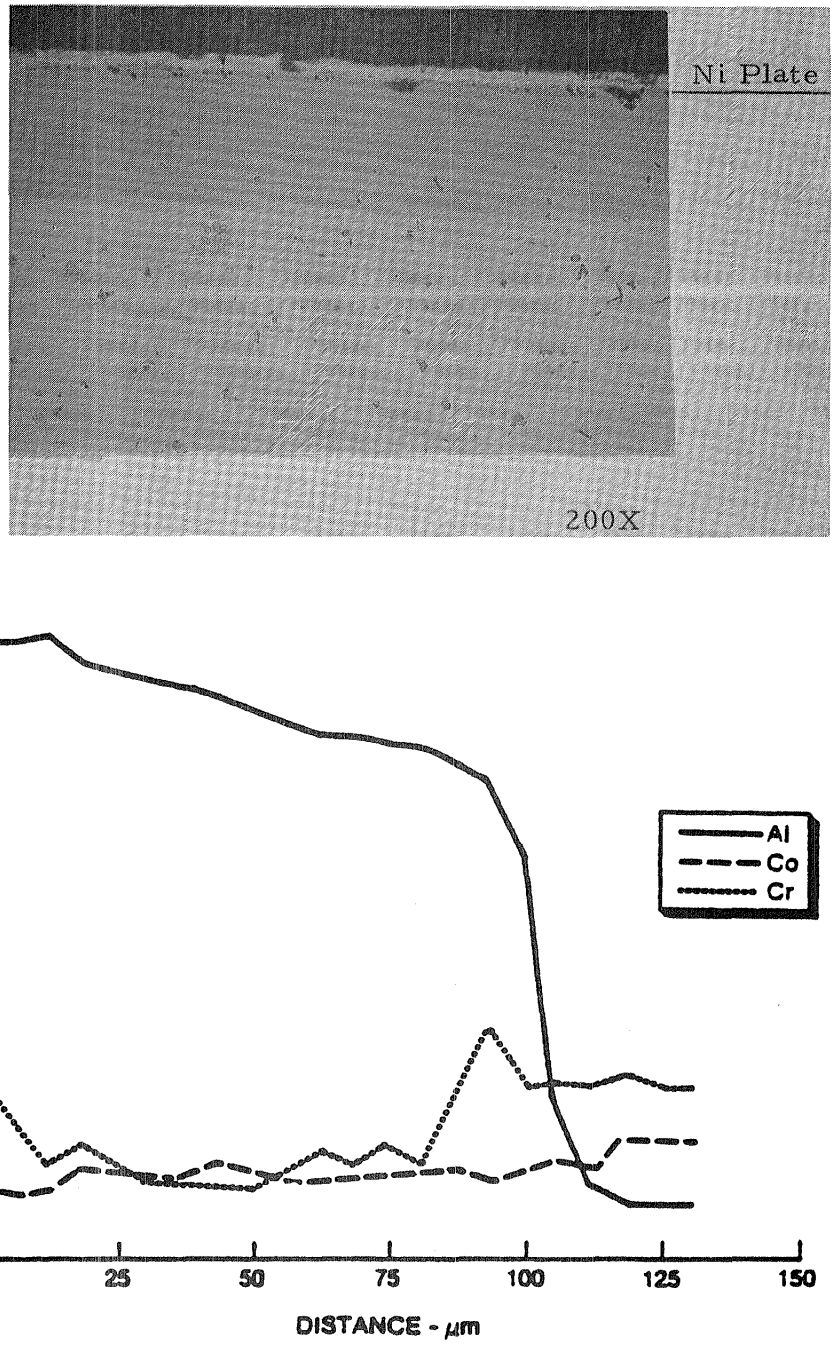

Figure 11 Microstructure and Microprobe Profile of 701 Aluminide Coating.

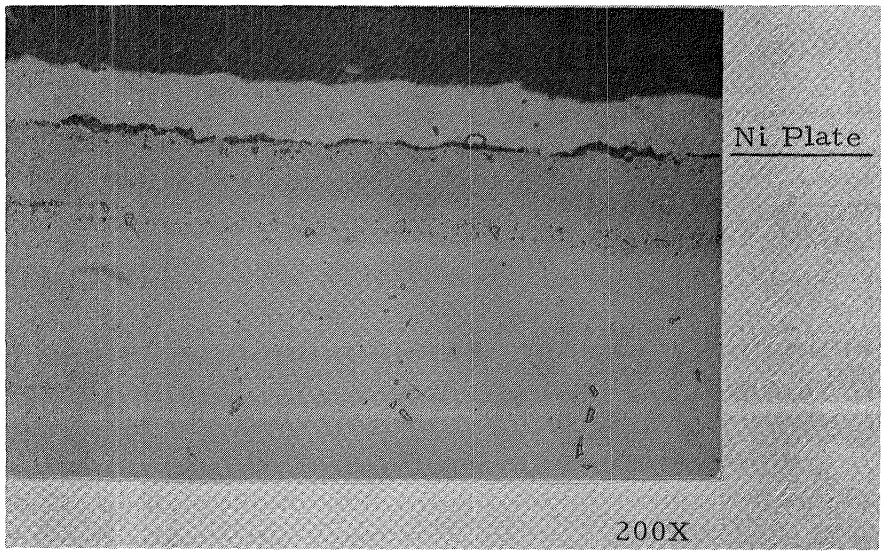

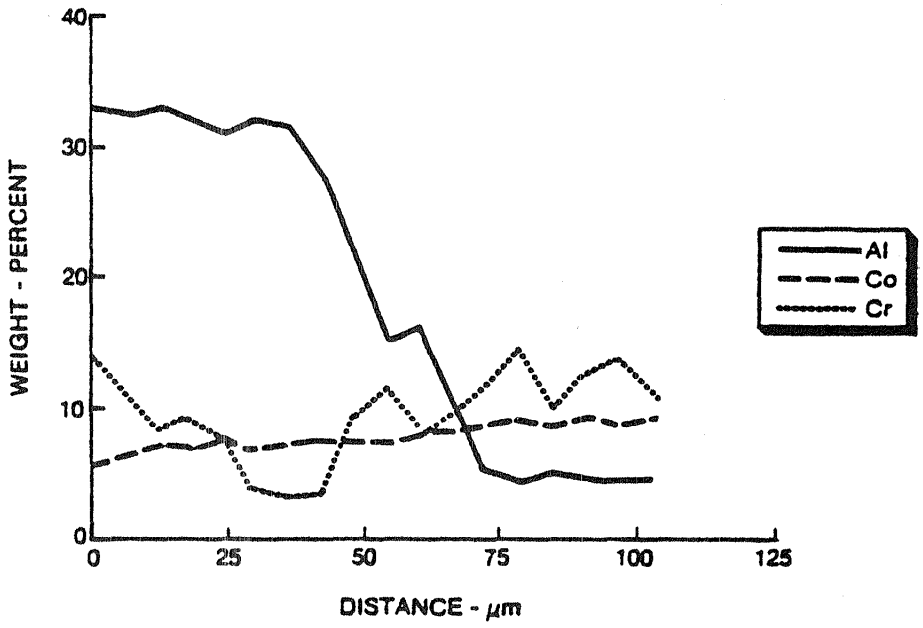

Figure 12 Microstructure and Microprobe Profile of MOD. 701 Aluminide Coating.

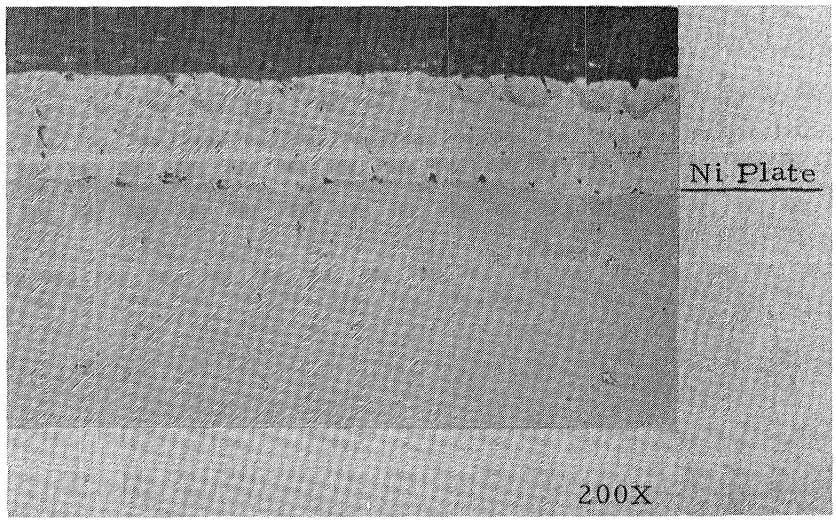

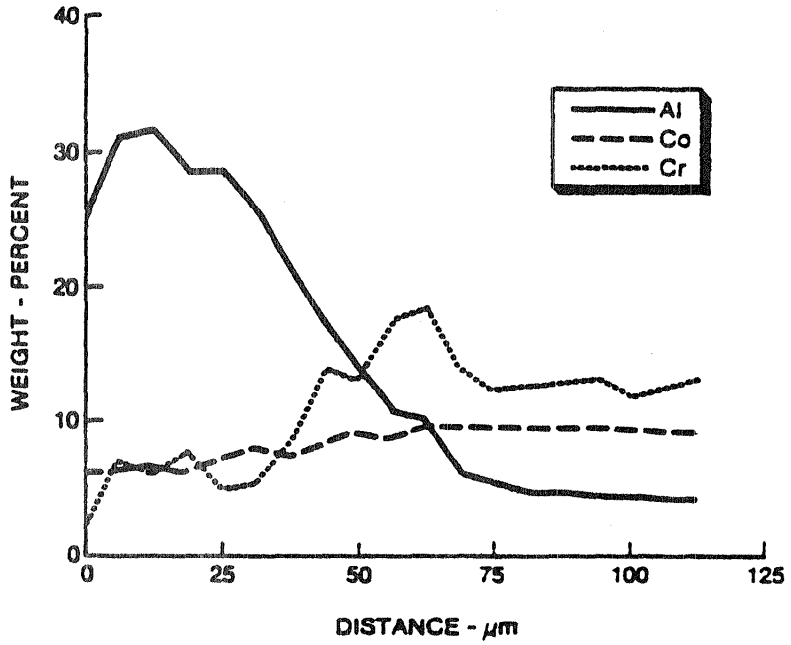

Figure 13 Microstructure and Microprobe Profile of RT21 Aluminide Coating.

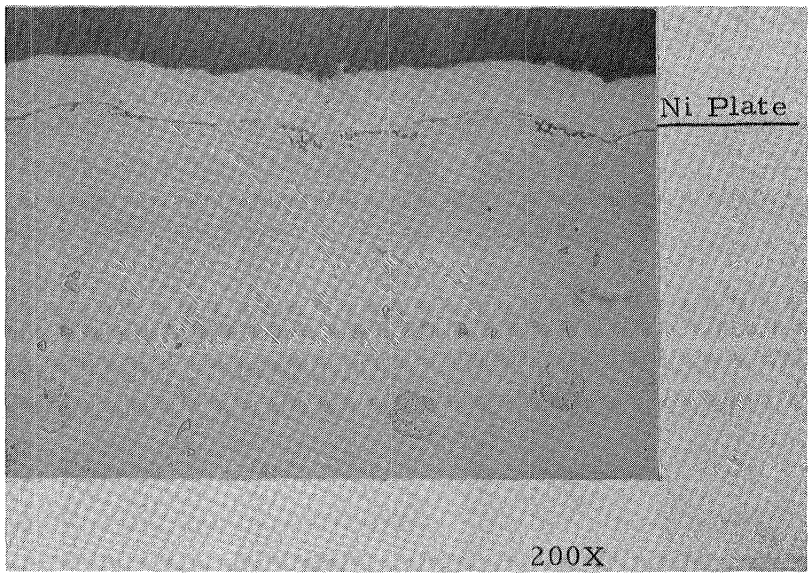

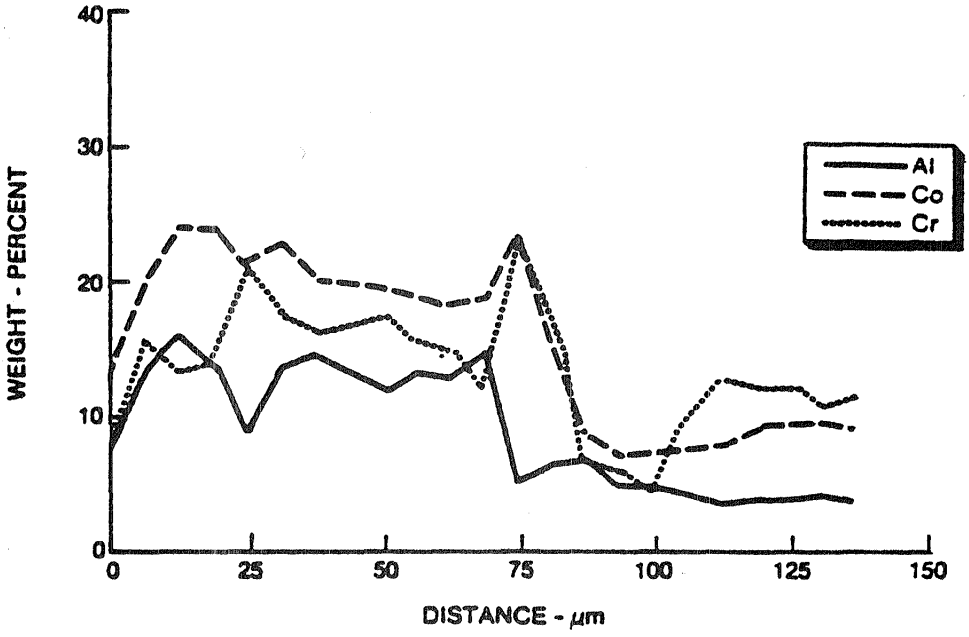

Figure 14 Microstructure and Microprobe Profile of Plasma Sprayed M3958 Coating.

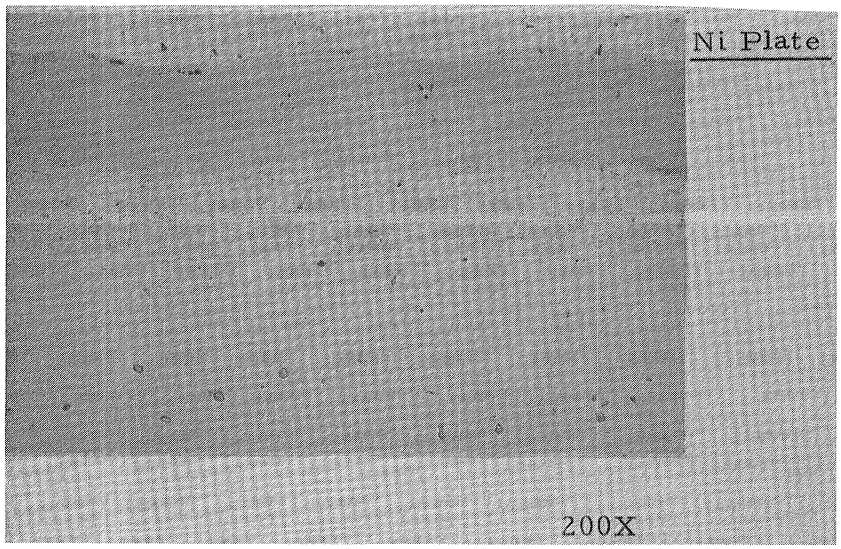

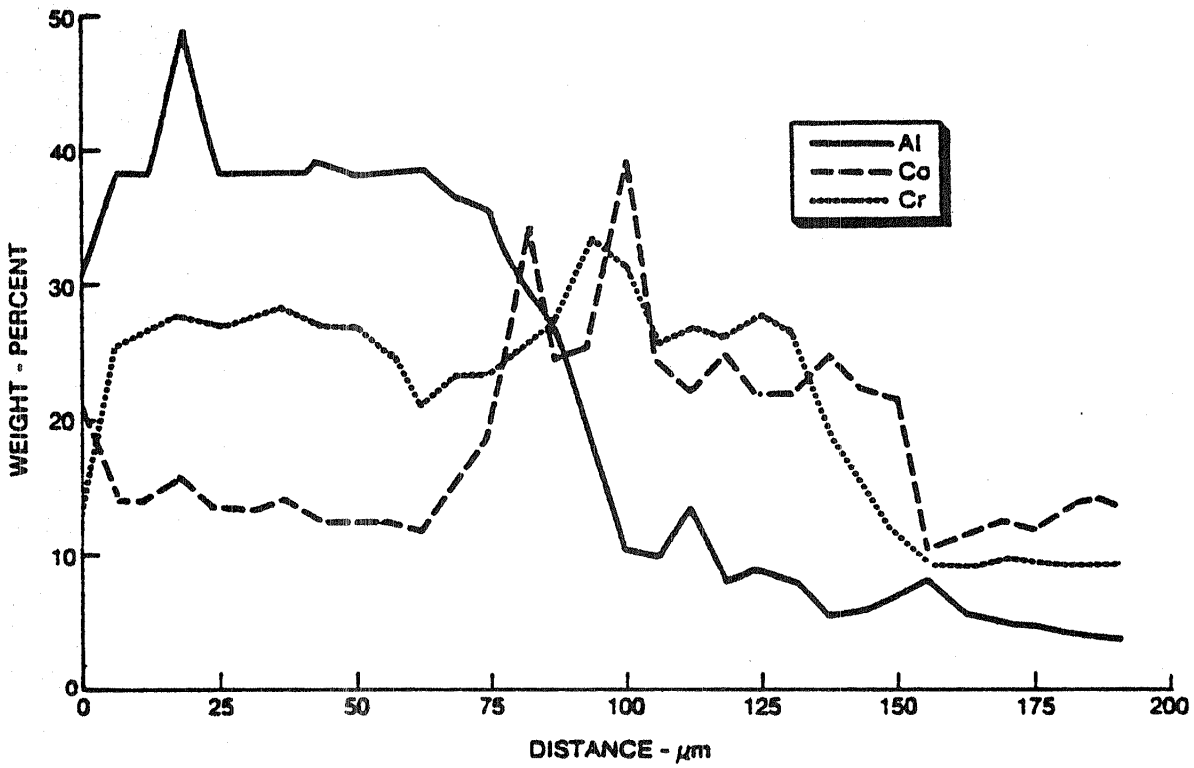

Figure 15 Microstructure and Microprobe Profile of M3959 + 701 Coating System.

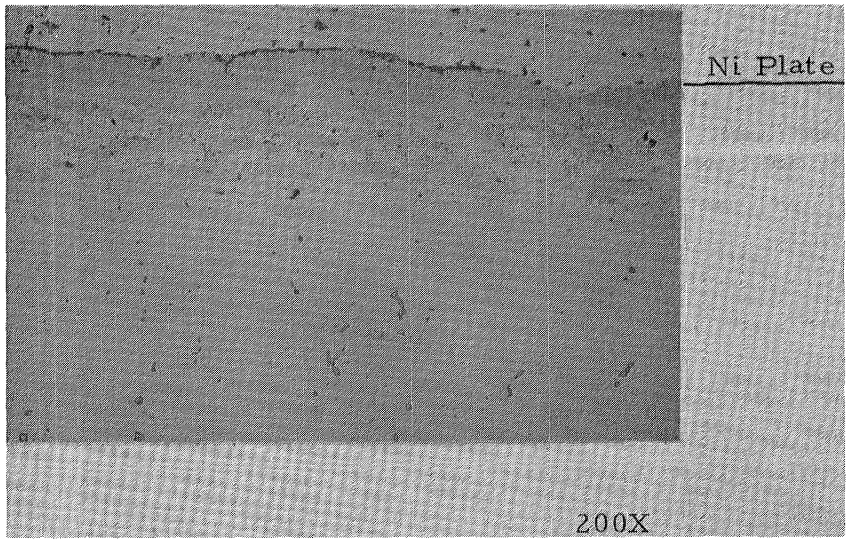

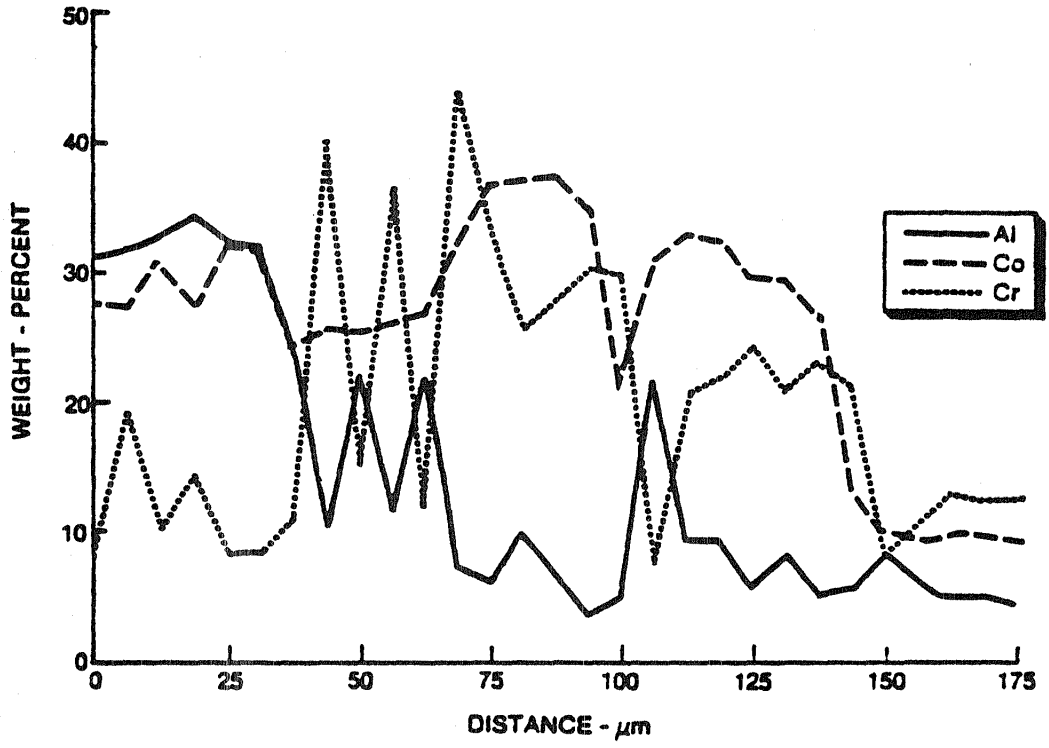

Figure 16 Microstructure and Microprobe Profile of M3959 + MOD. 701 Coating System.

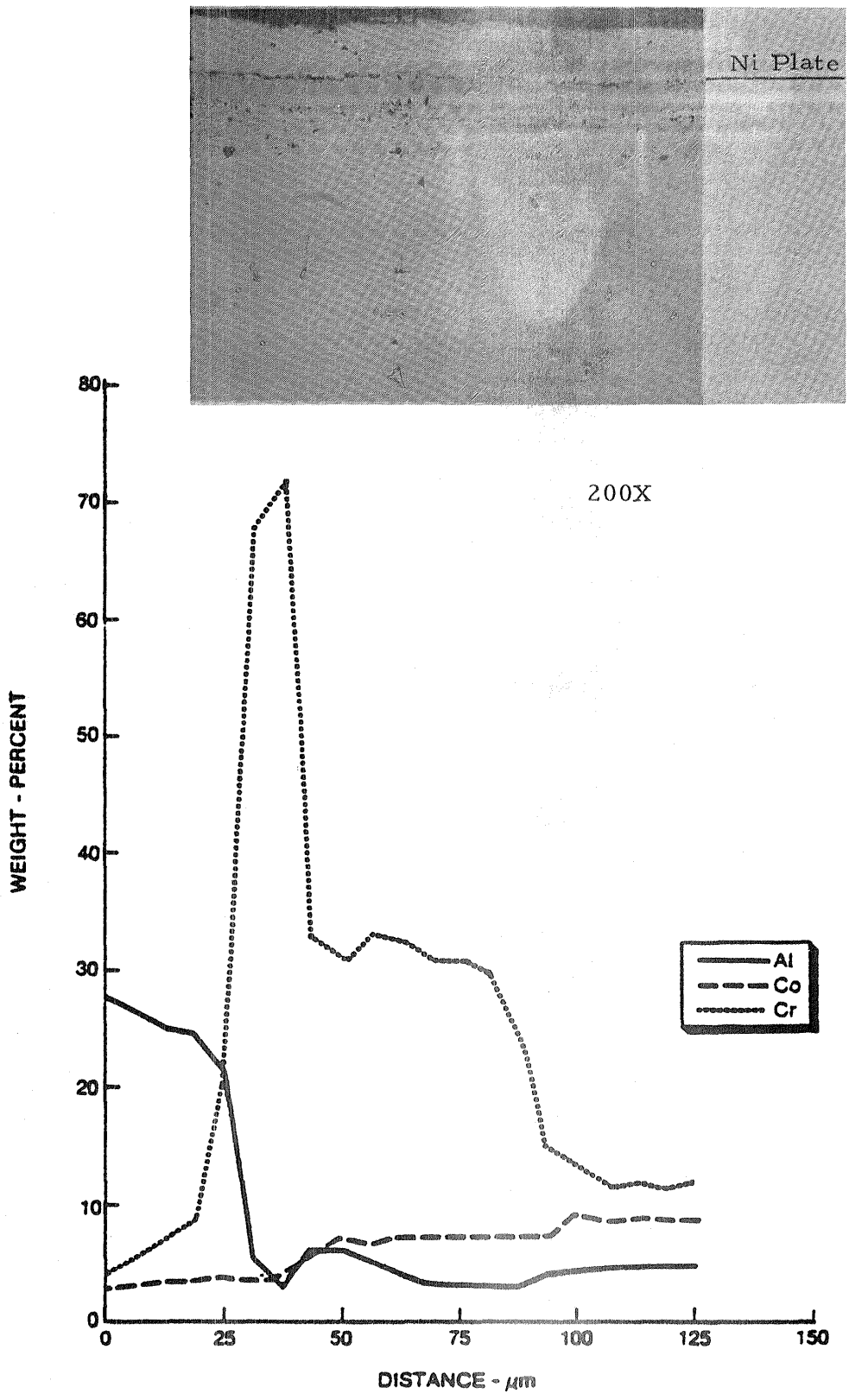

Figure 17 Microstructure and Microprobe Profile of M39AA + RT21 Coating System.

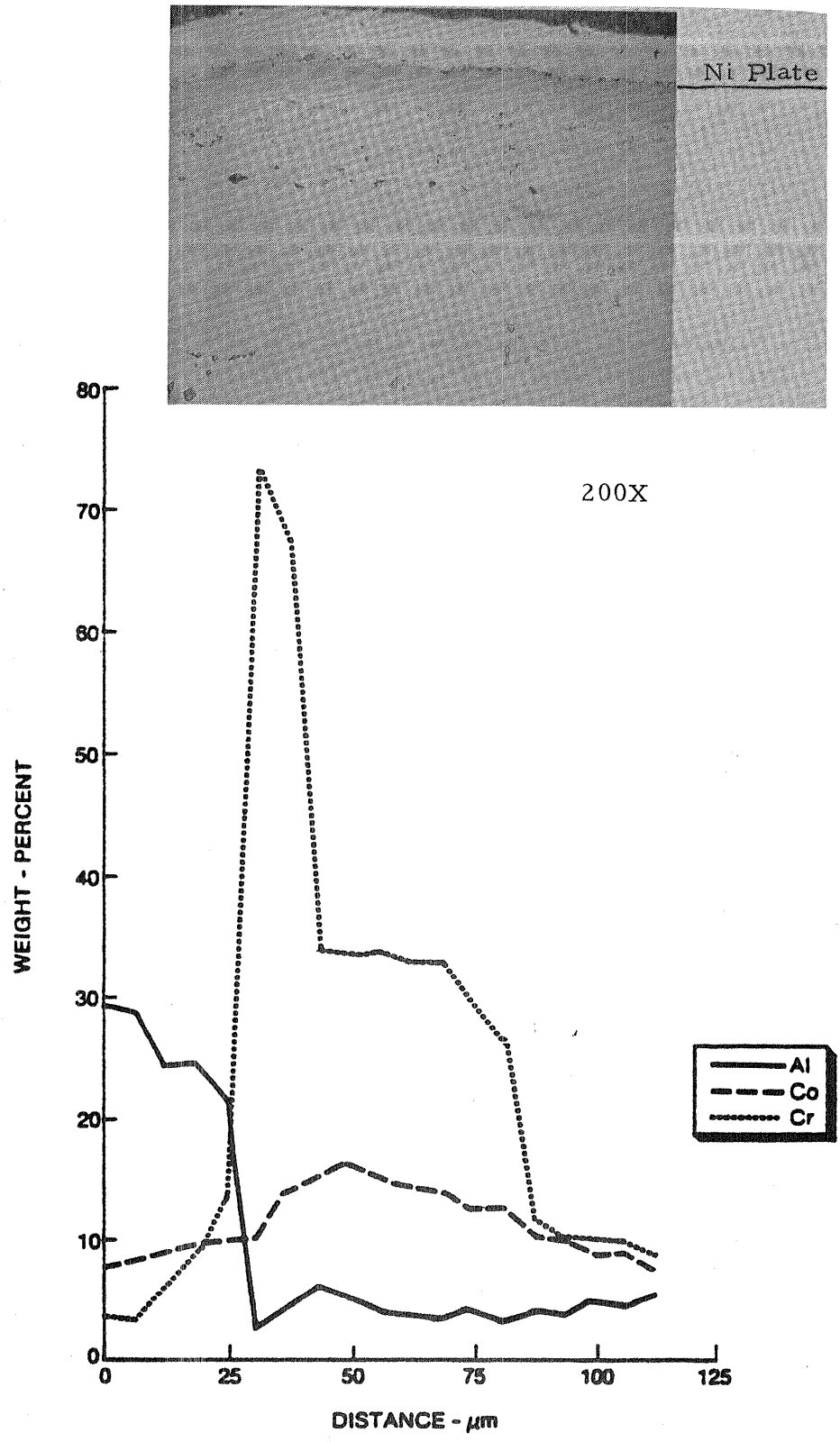

Figure 18 Microstructure and Microprobe Profile of M39AB + RT21 Coating System.

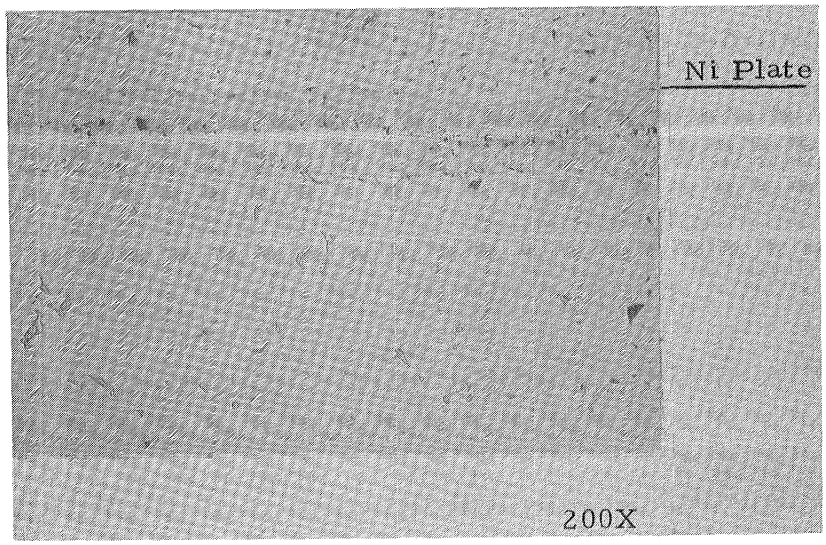

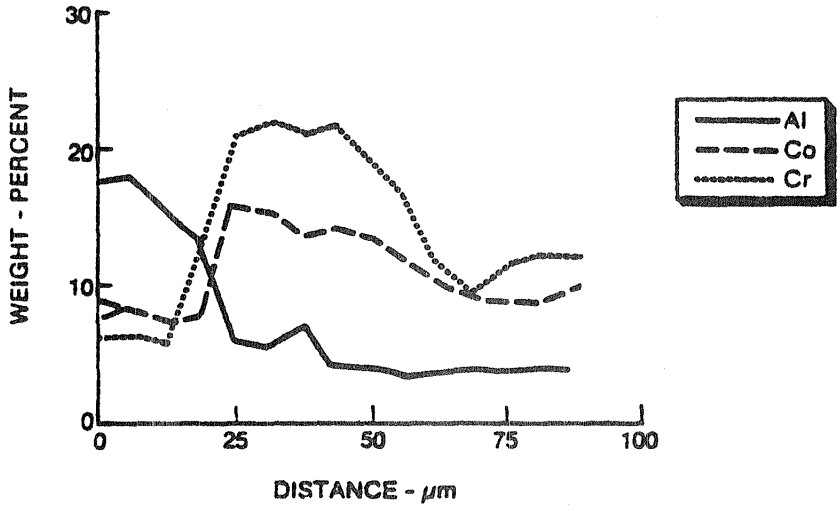

Figure 19 Microstructure and Microprobe Profile of M39AC + RT21 Coating System.

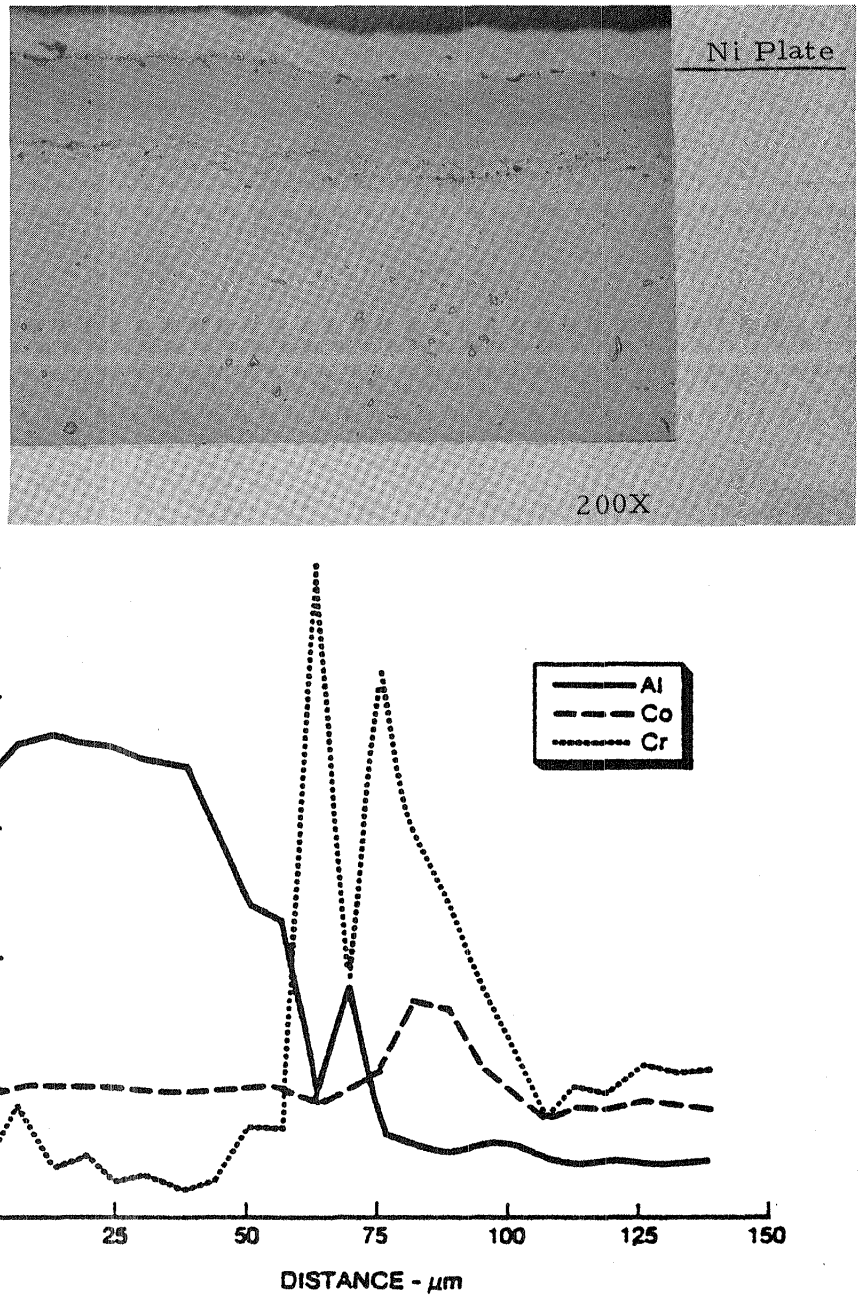

Figure 20 Microstructure and Microprobe Profile of M39AC + MOD. 701 Coating System.

of the coating (Figure 13).

b) Baseline Plasma Spray Coating

The M3958 plasma sprayed system had an average coating thickness of 76μm and a dense microstructure. (Figure 14). The coating had the typical dual phase structure ($\beta+\gamma'$) of a NiCoCrAlY coating. The aluminum concentration in the coating was 12 wt.%.

c) Plasma Spray CoNiCrAlY (6% Al) + Aluminide

The elemental microprobe profile and microstructure of M3959 (Co-29Ni-26Cr-6Al-.6Y) with two different aluminide (701 & Mod. 701) overcoats is shown in Figures 15 and 16. Comparison of the probe profiles of the NiCoCrY + Aluminide and the 6% Al-CoNiCrAlY + Aluminide coating systems reveal a significant difference. The presence of aluminum in the plasma sprayed undercoat seems to enhance the interdiffusion of various elements (especially Co and Al with Cr to a lesser extent) between M3959 and the aluminide overcoat which results in a graded coating (compare Figures 15 and 16 with 17 and 20).

d) Plasma Spray NiCoCrY + Aluminide

Metallographic investigation of the NiCoCrY + Aluminide Systems (M39AA + RT21, M39AB + RT21, M39AC + RT21, M39AC + Mod. 701) revealed a predominantly single phase β (NiAl) structure in the outer zone with a chromium rich layer just underneath the β layer. (Figures 17-20). This indicates that during the aluminizing or subsequent diffusion process, nickel from the plasma sprayed NiCoCrY diffused outward to react with the incoming aluminum to form the stable NiAl layer with its solid solution elements. The outward movement of nickel results in a region of high chromium content underneath the β layer. It is possible that this chromium-rich layer could also act as a diffusion barrier and prevent the aluminum from diffusing throughout the plasma sprayed NiCoCrY coating thickness. The inner zone of

these coating systems corresponds to a nickel deficient plasma spray composition of the undercoat (M39AA, M39AB) except for the chromium-rich layer at the aluminide-plasma coating interface.

The NiCoCrY + Aluminide systems exhibited voids at the plasma coating/substrate interface, plasma coating/aluminide interface and within the plasma sprayed region. A possible mechanism for void formation could be the presence of microscopic porosity in the as-plasma sprayed coating which acts as sinks for the vacancies in the Kirkendal mechanism of interdiffusion between the various elements during the aluminizing and or the diffusion heat treat process.

4.2 Thermal Fatigue Evaluation

4.2.1 Crack Growth Rate Data

The optically measured average crack lengths of the three largest cracks as a function of accumulated cycles are itemized in Appendex A for the 10 coating systems. All crack length data were measured on the small radius (R=0.635 mm) of the wedge specimen. Since the main objective of the program was to rank the performance of the various coatings based on coating crack initiation, the wedge specimens were inspected at regular intervals (100-150 cycles) at 30X and the crack lengths and the total number of cracks were recorded. Each crack was identified relative to location on the specimen by referencing it to the distance from the top end. The length of the cracks were measured along both the front and the back surfaces of the specimen. These were then averaged for each of the three largest cracks. The average crack length of the three largest cracks and the total number of cracks observed as a function of accumulated cycles give a measure of the crack growth data and the susceptibility of the coating system to thermal fatigue cracks. The number of cycles for coating crack initiation was calculated by averaging the number of cycles between the last inspection period when no crack was observed and the inspection period when the first crack was visible.

Initial testing was conducted using the cycle described in Figure 7 which used a quench water flow rate of 18 gm/sec. It became obvious that this cycle was too severe as it failed the specimens rapidly and provided insufficient discrimination. Subsequent testing was conducted with a lower water flow rate (10.5 gm/sec). However, due to sample and schedule time availability, retesting of the first group could not be accomplished. Therefore, a correction factor was introduced by utilizing the test results for the RT21 and 701 coated specimens. A correction factor of + 150 cycles was applied to the initial test group (fast quench rate, Table A-1) when this data was used for comparison purposes with the slower quench rate cycle specimens (Table A-2).

Table 3 summarizes the crack initiation data and the number of cracks after 1050 cycles. The data for the fast quench cycle specimens (identified with an asterisk) has been corrected to the slow quench cycle so that all coating systems in Table 3 can be compared on an equal basis, ie. the slower quench rate cycle. From these results, the coating systems are ranked into four groups (I-IV) according to performance. This ranking is also shown graphically in Figure 21. At the conclusion of rig testing, one specimen from each coating system was stripped of its coating and the average crack lengths of the three largest cracks and the total number of cracks was remeasured by optical examination. The purpose of remeasuring the cracks after stripping the coating was to compare with the crack lengths before stripping and verify, if indeed, the cracks had penetrated through to the substrate or were just surface cracks in the coating. Specimens which had the most accumulated cycles were used for stripping. Table 4 contains the summary of the calculated average crack lengths of the 3 largest cracks and the total number of cracks observed before and after stripping the coating for comparison purposes. The total

TABLE 3: Summary of Slow Quench Cycle Thermal Fatigue Test Data.

Sp. No.	Coating Type	Cycles to Crack Initiation	Number of Cracks After 1050 Cycles	Coating Group Classification (Arbitrary)
A38	701	675	1	Group II
A39	Mod. 701	675	3	Group II
A10	RT21	375	16	Group IV
A7	M3958	975	1	Group I
A3 A9	M3959 + 701	600+	3+	Group II
A5 A13	M3959 + Mod. 701	600+	1+	Group II
A34	M39AA + RT21	400*	23	Group IV
A30	M39AB + RT21	400*	30	Group IV
A19	M39AC + RT21	500*	12	Group III
A23	M39AC + Mod. 701	525	1	Group III

* Fast quench cycle data corrected to slow quench cycle.

\+ Averaged values.

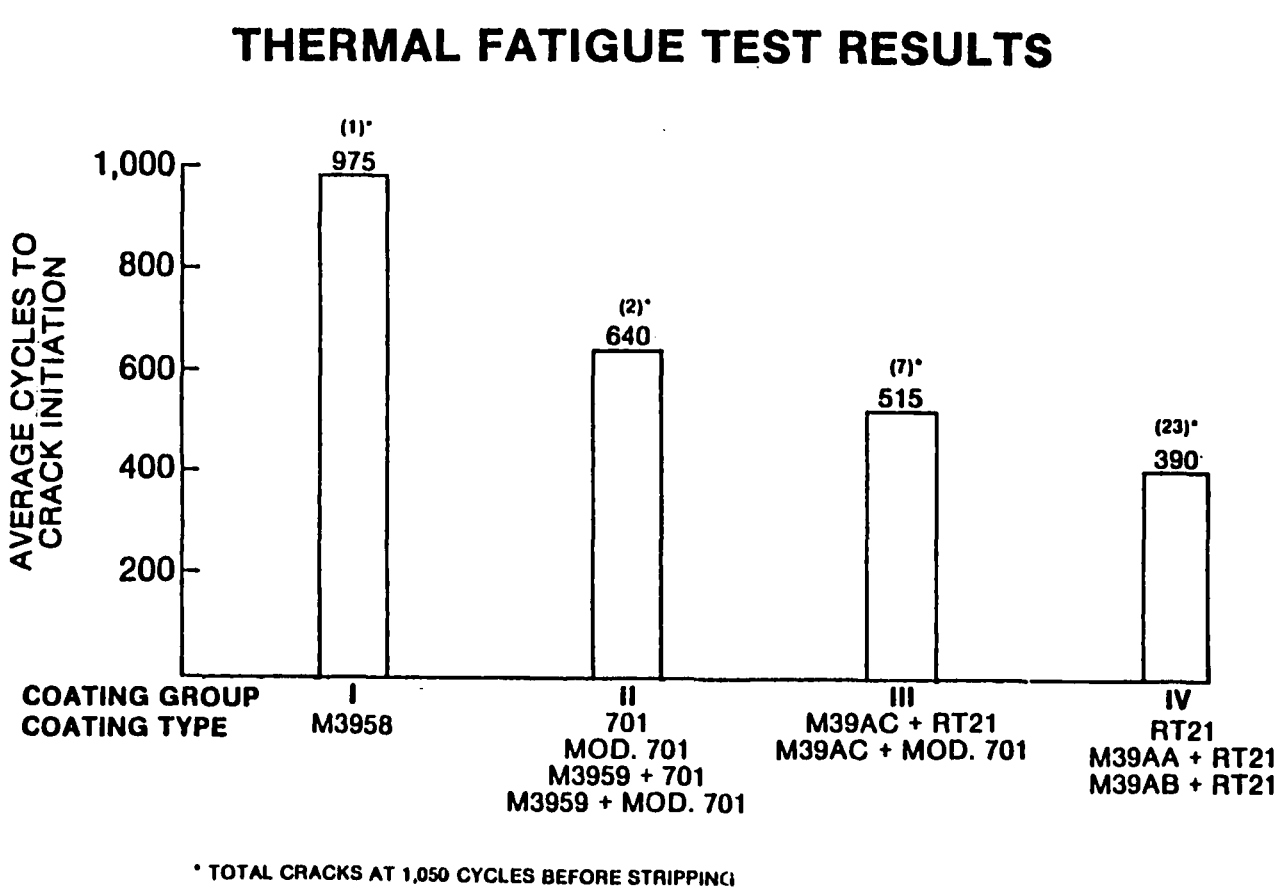

Figure 21 Relative Performance of Various Coatings in Thermal Fatigue Based on Cycles to Crack Initiation and Total Number of Cracks.

TABLE 4: Summary of Crack Length Data Before and After Stripping the Coating at Termination of Thermal Fatigue Test.

Sp. No.	Coating System	Total Test Cycles[1]	Before Stripping		After Stripping	
			Average of (3) Largest Cracks, mm.	Total Cracks Observed	Average of (3) Largest Cracks, mm.	Total Cracks Observed
A38	701	1500	2.7	4	—	—
A38	701	2250	3.81	7, cc.	3.68	16, cc.
A39	Mod. 701	1500	3.42	5, cc.	3.42	10, cc.
A10	RT21	1050	3.38	16, cc.	3.00	16, cc.
A7	M3958	1500	2.2	2	2.2	2
A3	M3959 + 701	1500	3.76	22, e.	3.85	24
A13	M3959 + Mod. 701	1500	3.76	2, cc.	3.85	3, cc.
A34	M39AA + RT21	1050*	4.31	23, cc, s.	3.42	3
A30	M39AB + RT21	1050*	2.11	30, e, s.	1.26	4
A19	M39AC + RT21	1050*	2.53	12	2.32	2
A23	M39AC + Mod. 701	1500	3.46	3, cc.	3.08	2

1. Test Cycle-Figure 7; cc = crazing cracks; e = eruption; s = spall
* Fast quench cycle data corrected to slow quench cycle.

number of cracks that were observed after 1050 cycles (before stripping) are also noted for groups I-IV in Figure 21. It is apparent that cycles to crack initiation and the total number of cracks are consistant criteria for ranking performance.

Figure 22 shows the appearance of the wedge specimens of some typical coating systems after the coating was stripped at the termination of slow quench cycle thermal fatigue test. Note the presence of the craze crack patterns on the substrate of the specimens after the aluminide (specimens B and C) coating was stripped indicating the brittleness of the system. The surface of the M3958 (12% Al-NiCoCrAlY) was smooth except for the crack which had penetrated into the substrate. A comparison of the visual substrate appearance of the M3958 and Mod. 701 (specimens A and C) after the coating was stripped indicates the superior ductility of the M3958 (no craze crack patterns) compared to the aluminide when tested to the same number of cycles (1500). Closer examination of specimen D [M3959 (6% Al-CoNiCrAlY) + Mod. 701] indicates a mild crazing pattern on the substrate of the specimen after the coating was stripped. As explained previously, this could mean that a better bond existed between the Mod. 701 and the M3959 layer (also see Figure 16) which transmitted the craze crack pattern from the aluminide to the substrate through the M3959 layer. This would also indicate that the overall coating system would be brittle in nature as was evidenced by the crack length data for the M3959 + Mod. 701 system.

The M3958 (Group I) coating outperformed all other groups of coatings by a factor between 1.4 to 2.5 in crack initiation. The M3958 also exhibited the slowest crack growth rate (Appendix A). Typically the average calculated crack length for this coating was 2.2 mm at 1500 cycles compared to 3.4 mm for Group II coatings. Additionally, the total number of cracks recorded for the M3958 (Group I) coating was the lowest compared to the other groups, indicating it to be the most thermal fatigue resistant coating.

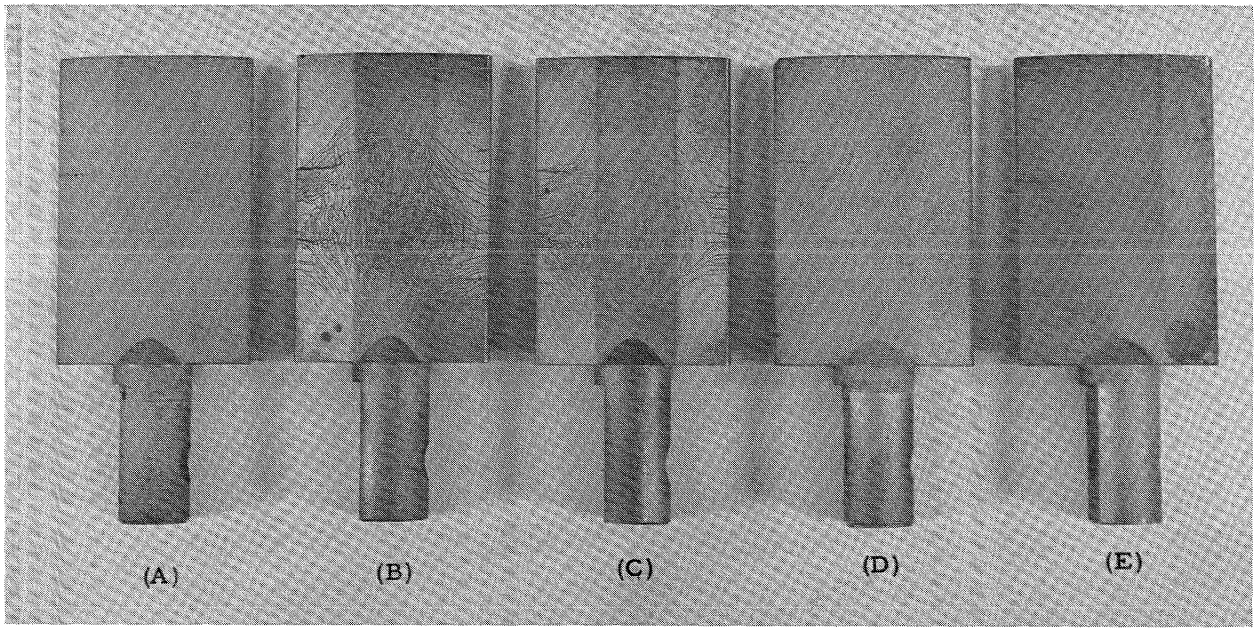

Figure 22 Appearance of Thermal Fatigue Wedge Specimens After Stripping the Coating at Termination of Slow Quench Cycle Test.
A: M3958 (1500 cycles B: 701 (2250 cycles)
C: MOD. 701 (1500 cycles) D: M3959 + MOD. 701 (1500 cycles)
E: M39AC + MOD. 701 (1500 cycles)

Within the Group II coatings (701, Mod. 701, M3959 + 701 and M3959 + Mod. 701), the Mod. 701 coating system indicated a faster growth rate than the 701 coating (compare specimens A38 and A39 in Table 4 at 1500 cycles), although both systems recorded the same number of cycles at the crack initiation. This would seem to indicate that lowering the aluminum content (from 40 w/o for 701 to 32 w/o for Mod. 701) does not necessarily "ductilize" the aluminide layer and that NiAl exhibits similar cracking characteristics in its hyperstoichiometric (Al content > 31.48 w/o) range. The M3959 (6% Al-CoNiCrAlY) + 701 coating exhibited eruptions and spallation of the outer aluminide once the coating crack was initiated while this behaviour was not observed for the M3959 + Mod. 701 coating. The M3959 + aluminides exhibited similar fatigue cracking characteristics as the Mod. 701, although the crack growth rate was slightly faster (see Table 4). This could be due to the effects of the cobalt based MCrAlY in the coating system. Since a nickel based MCrAlY is generally more ductile than its cobalt based counterpart, further investigation should trend towards evaluating the effects of 6% Al-NiCoCrAlY + aluminide coating system.

A comparison between the performance of Group I and Group III (M39AC + RT21, M39AC + Mod. 701) coatings (see Figure 21) indicates the superiority of Group I (M3958) coating by a factor of 1.9. Amongst the NiCoCrY + RT21 systems, the M39AC (Ni-15Co-20Cr-.6Y) + RT21 (Group III) exhibited slightly superior performance in thermal fatigue cracking when compared with M39AA + RT21 and M39AB + RT21 in Group IV. Both the M39AA + RT21 and M39AB + RT21 exhibited numerous closely spaced cracks, with spalling of the outer high aluminum content layer. Despite its lower aluminum content (25 w/o) compared to the 701 coatings (32 - 40 w/o), the RT21 aluminide (Group IV) exhibited relatively poor thermal fatigue crack initiation characteristics when compared with the Group II (701, Mod. 701) aluminides.

Except for the NiCoCrY + aluminide systems, the crack length data after stripping agree reasonably well with the data before stripping for the other systems. This would indicate that the cracks did penetrate the substrate. The craze crack patterns which were present on the aluminide systems at completion of tests was also present on the substrate after the coating was stripped. An appreciable difference was noticed in the calculated average crack length after stripping for the M39AA + RT21 and M39AB + RT21 systems.

As both these systems (high Cr-NiCoCrY + aluminide) had exhibited spalls and eruptions during testing, it would indicate that the bond between the aluminide and the underlayer (M39AA or M39AB) was not adherent and that the cracks occurred primarily on the high aluminum content layer. The closely spaced cracks observed after the completion of testing were not present after stripping, indicating that they were surface cracks in the outer aluminide layer. The M3959 (6% Al-CoNiCrAlY) + 701 system, which also exhibited eruptions and closely spaced cracks at completion of test, did show some indications of numerous mild cracks along the edge radius after stripping. This indicates a better bond between the plasma sprayed undercoat and the aluminide overcoat during the initial stages of testing. However spalling of the outer aluminide layer did occur after 1000 cycles. The M39AC (low Cr-NiCoCrY) + aluminide systems did not exhibit a sharp drop in the cummulative crack length measurement after the coating was stripped and followed a similar trend as the plain aluminide systems. However the craze cracks and the numerous closely spaced cracks observed on the surface of the coatings before stripping were not visible after the coating was stripped. This would indicate that either the ductile underlayer of M39AC absorbed the craze cracks or the coating cracks were concentrated in the aluminide layer and were not transmitted to the underlayer because of separation between the RT21 and M39AC layer. The latter seems the more likely

possibility since porosity/voids were present in the M39AC + RT21 (see Figure 34) coated specimen at the interface between the aluminide-plasma spray surface after thermal fatigue testing.

4.2.2 Metallurgical Evaluation of Fatigue Cracks

A metallographic examination was performed to establish the nature and extent of the fatigue cracks on the specimen within each coated system which showed the lowest life. Essentially, the specimens were sectioned around the region of the cracks on the small edge radius and a longitudinal section was metallurgically examined. The cracks were primarily intergranular in nature. The crack lengths which were measured by metallographic examination agreed well with those measured by optical examination.

Figures 23 and 24 show the typical intergranular nature of crack propogation. Figure 23 shows the nature of cracks for a 701 (40 w/o Al) aluminide at 800 cycles while Figure 24 shows the crack propogation for RT21 (25 w/o Al) aluminide at 650 cycles. A comparison of the cracks which occured in the Mod. 701 (32 w/o Al) aluminide and an RT21 aluminide (Figures 25 and 26) show the similar nature of the cracks. The calculated average crack length at 650 cycles for the RT21 coated specimen was twice as large when compared with the 701 coated specimen (sp. nos. A8 and A36) indicating that different stress levels may act at the aluminide-substrate interface for the two systems.

The microstructure of the M3958 (12% Al-NiCoCrAlY) coated specimen at 650 cycles is shown in Figures 27 and 28. Recent work (Ref. 6) conducted at NASA Lewis Research Center on thermal fatigue cracking of various coatings on wedge specimens of IN-792 + 1% Hf alloy indicated an improvement in cycles to crack initiation of M3958 over 701 by at least a factor of 2 compared to 1.44 in this study. This discrepancy can be attributed to the increased severity of our test cycle which employed a water jet quench for thermal shock while the NASA test utilized the IITRI fluidized bed technique.

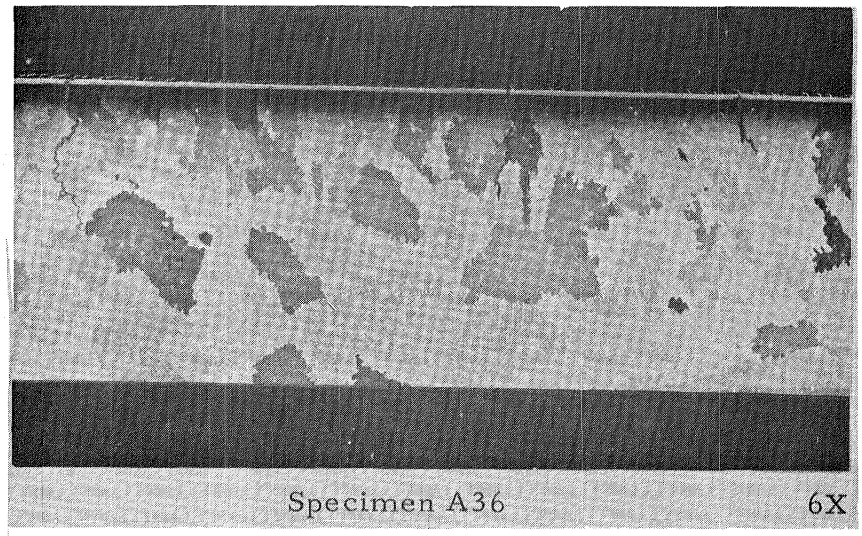

Figure 23 Microstructure of 701 Coated Specimen showing Intergranular Nature of Thermal Fatigue Cracks after 800 Cycles of Test.

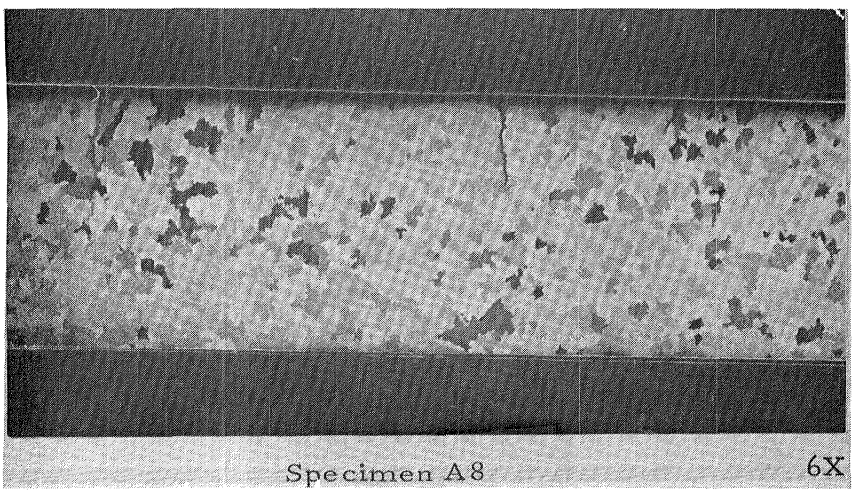

Figure 24 Microstructure of RT21 Coated Specimen Showing Intergranular Nature of Thermal Fatigue Cracks after 650 Cycles of Test.

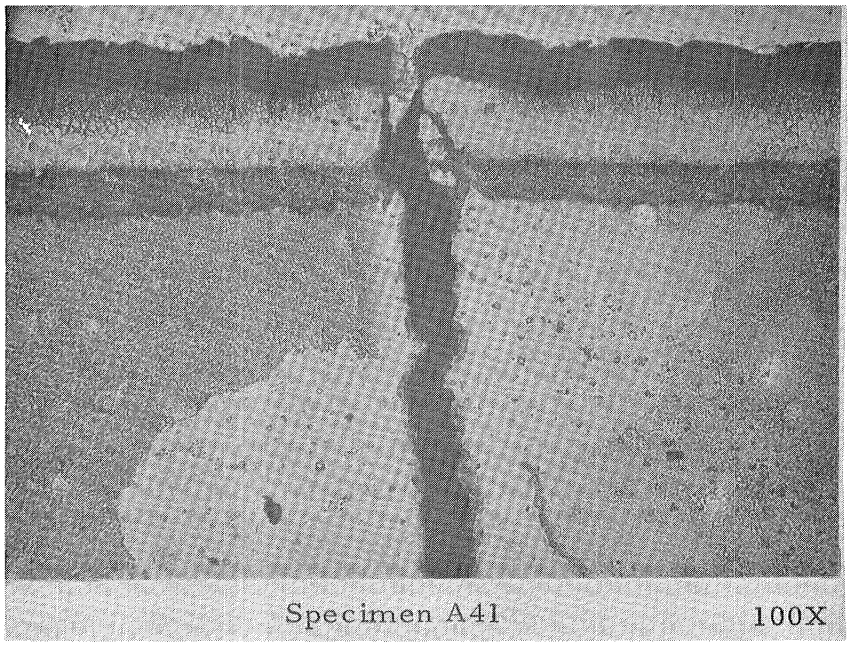

Figure 25 Close-Up of Thermal Fatigue Crack in MOD. 701 Coated Specimen after 1050 Cycles of Test.

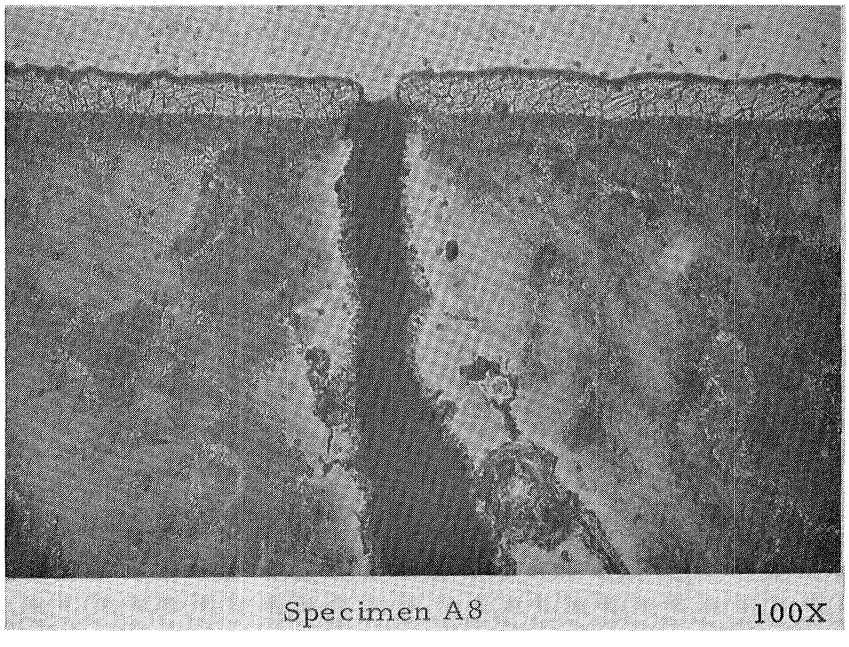

Figure 26 Close-Up of Thermal Fatigue Crack in RT21 Coated Specimen after 650 Cycles of Test.

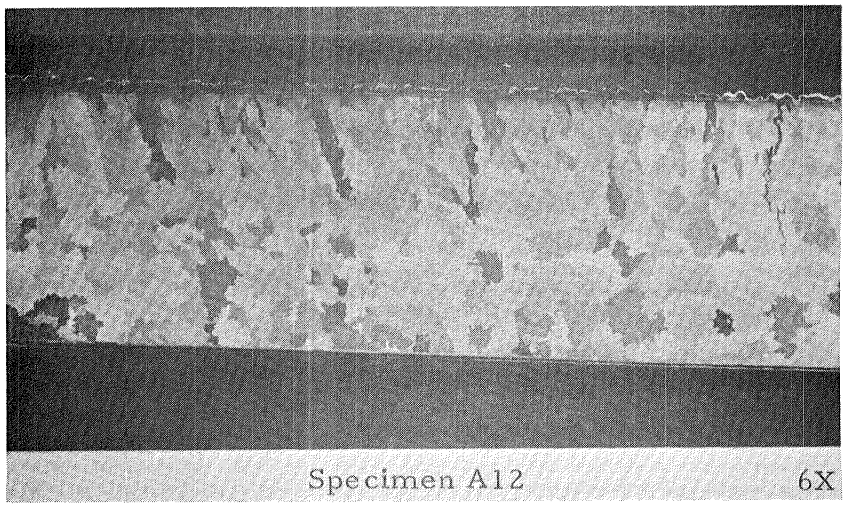

Figure 27 Microstructure of M3958 Coated Specimen after 650 Cycles of Thermal Fatigue Test.

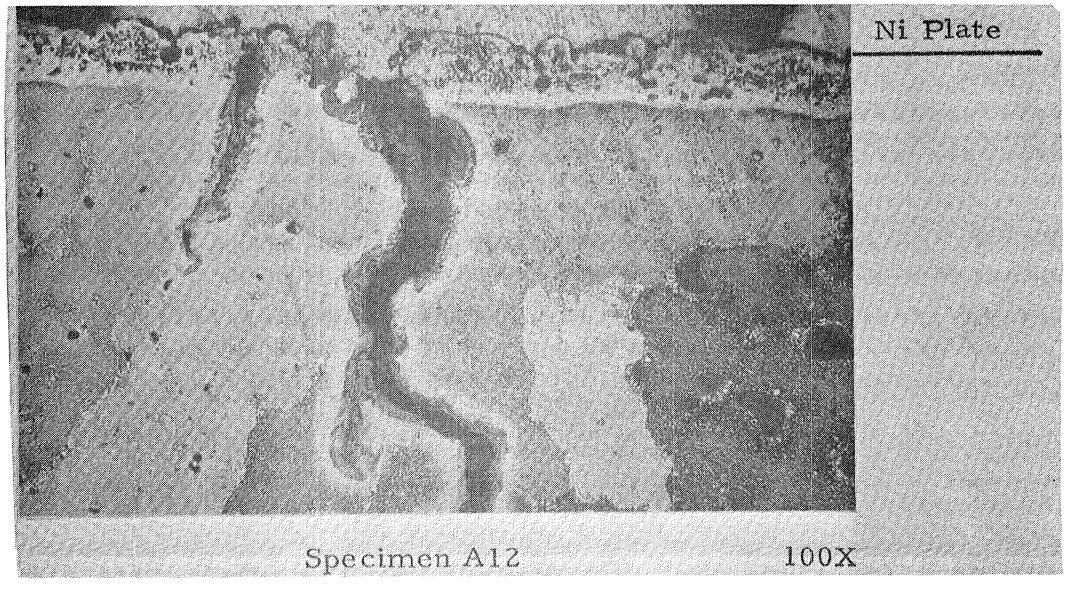

Figure 28 Close-Up of Thermal Fatigue Crack in Figure 27.

A cross-section showing the nature and extent of the fatigue cracks in the M3959 (6% Al-CoNiCrAlY) + Mod. 701 coated specimen is shown in Figures 29 and 30. The close-up of the region near the largest crack in Figure 30 indicates that the crack originates in the aluminide and progresses through the M3959 underlayer with the final propogation through the substrate.

Metallurgical examination of the duplex systems involving a plasma sprayed NiCoCrY undercoat and an aluminide overcoat indicated a generalized failure mode of cracking in the aluminide combined with separation of the outer high aluminum content layer from the NiCoCrY underlayer. The separation of the outer aluminide layer occured to a higher degree for a high Cr (35 w/o) - NiCoCrY underlayer when compared with the low Cr (20 w/o) - NiCoCrY (M39AC) layer. Figure 31 represents a region where closely spaced cracks occurred in the outer aluminide layer of the M39AA (Ni-5Co-35Cr-.6Y) + RT21 coated specimen while Figure 32 illustrates a typical separation of the outer aluminide (RT21) from the M39AB (Ni-15Co-35Cr-.6Y) underlayer. Figures 33 and 34 show the nature of cracks for the M39AC (Ni-15Co-20Cr-.6Y) + RT21 Coated Specimen. It is apparent that for the duplex systems tested in this program, a combination of thermal expansion mismatch and voids due to accelerated diffusion between the outer high aluminum content layer and the NiCoCrY underlayer contributed to the spalling/separation of the outer aluminide. The trend for future development work of two-step (plasma spray + aluminide) coating systems should be directed towards a lower Cr content plasma underlayer to inhibit the Cr-rich layer formation at the plasma spray-aluminide interface after aluminizing. Likewise the objective of achieving a graded aluminum content in the plasma sprayed underlayer can be obtained by 1) utilizing a low aluminum content underlayer or 2) combining the NiCoCrY underlayer with a modified pack process resulting in the use of an "inward diffusion"

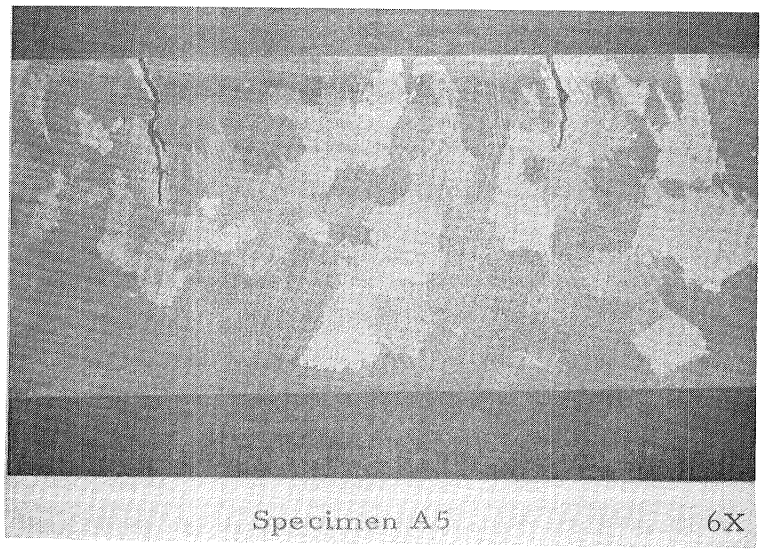

Figure 29 Microstructure of M3959 + Mod. 701 Coated Specimen Showing Morphology of Thermal Fatigue Cracks after 1050 Cycles of Test.

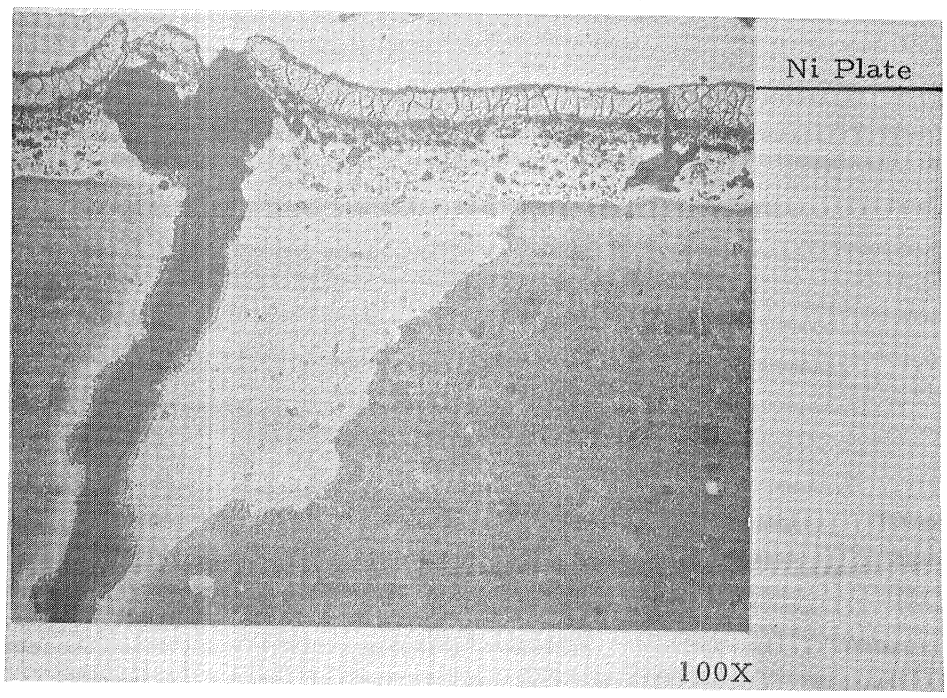

Figure 30 Close-Up of Largest Thermal Fatigue Crack from Figure 29.

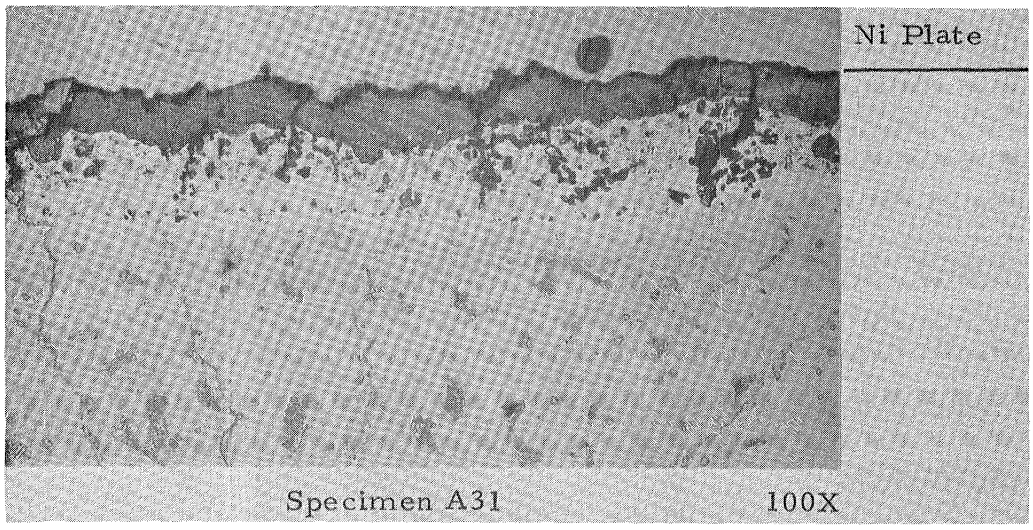

Figure 31 Close-Up of Thermal Fatigue Crack in M39AA + RT21 Coated Specimen after 900 Cycles of Test. Note Numerous Closely Spaced Cracks in the Outer RT21 Aluminide Layer.

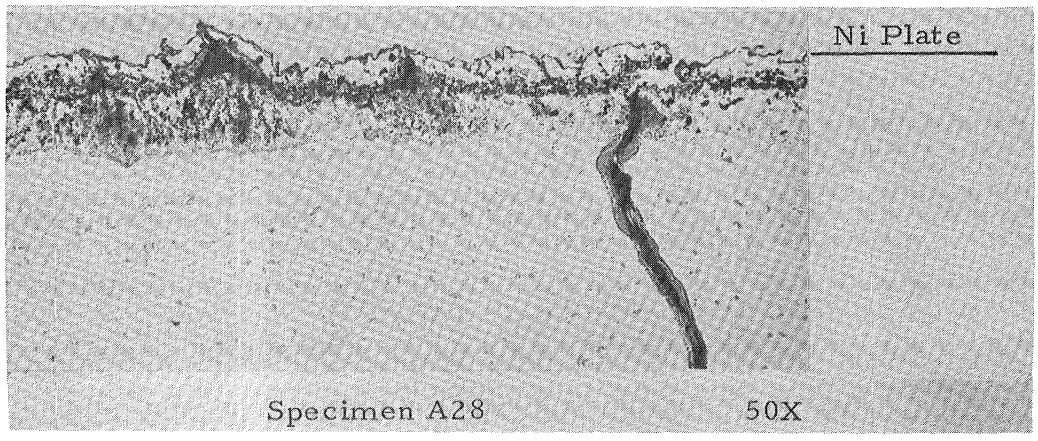

Figure 32 Microstructure of M39AB + RT21 Coated Specimen after 900 Cycles of Thermal Fatigue Test. Note Separation of Outer Aluminide Plasma Sprayed Undercoat.

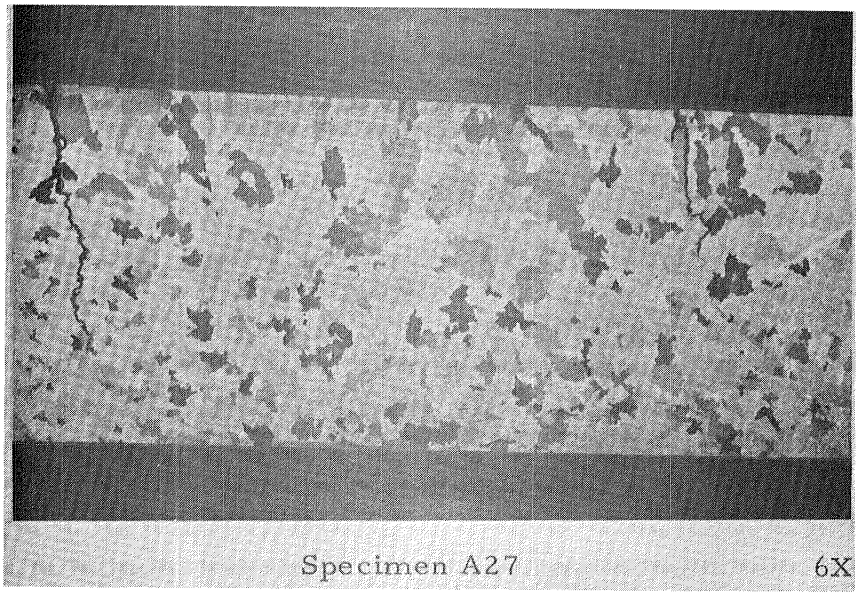

Figure 33 Microstructure of M39AC + RT21 Coated Specimen after 900 Cycles of Thermal Fatigue Test.

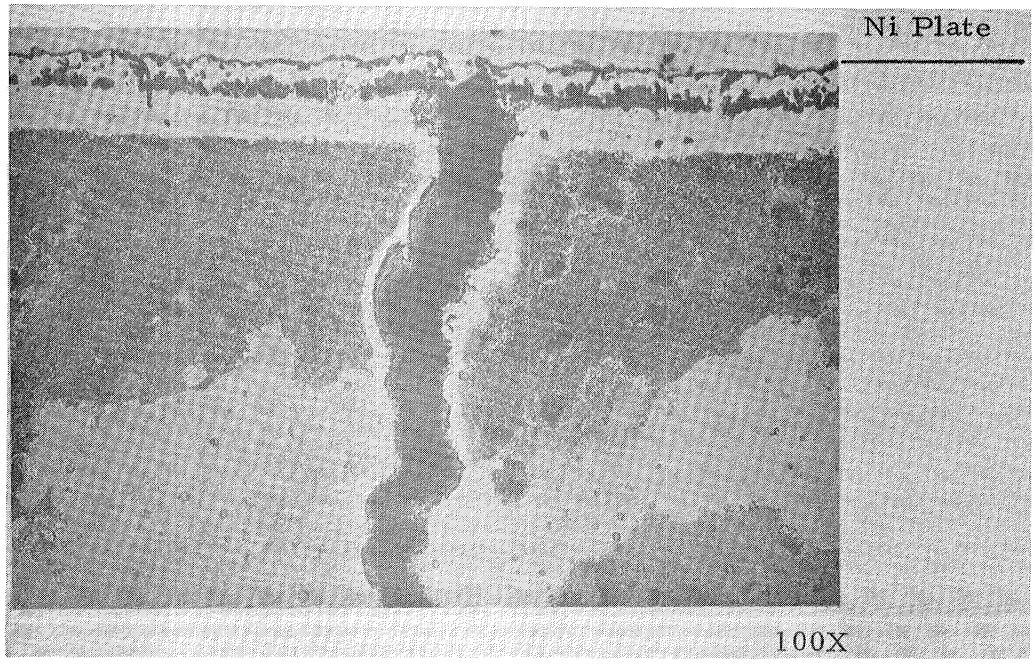

Figure 34 Close-Up of Largest Crack in Figure 33.

aluminide overcoat.

4.3 Oxidation/Corrosion Evaluation

The performance of the six coating systems exposed to the oxidation/corrosion cycle defined in Figure 9 was based primarily on visual observation of coating failure. Oxidation/corrosion occurs preferentially near the trailing edge region of the test paddles as these tend to be at higher temperatures. While spalling of the outer aluminide coating was observed in some NiCoCrY + RT21 coating systems, the criteria for coating failure was established as occurring when 0.1cm^2 or more of the substrate was exposed either due to coating spall or due to progressive coating degradation. The visual examinations and weight changes were made after every 20 hours. These results are tabulated in Table 5. The weight change was expressed in percent of the original weight since oxidation/corrosion was not uniform over the test specimen.

The relative ranking performance of the various coating systems was based on the normalized coating life expressed in minutes per micron of the coating thickness since the oxidation/corrosion life of the coating is usually proportional to its thickness. The coating thickness was based on the average of the pretest coating thickness of the Lycoming wedge metallographic specimen and the post test coating thickness at the top (colder region) section of the test paddle specimen. The failure point and the normalized coating lives for the six coating systems are given in Table 5, and graphically illustrated in Figure 35. Discussions of individual coating system performance and metallographic evaluation are given below.

The 701, M3958 and the M3959 + Mod. 701 systems failed by the usual corrosive attack through the protective surface caused by the gradual loss of aluminum content. The M3959 + Mod. 701 indicated the best performance in oxidation/corrosion resistance. Its coating life was greater than the

TABLE 5: Oxidation/Corrosion Data of Various Coating Systems on C101 Alloy.

COATING [a]		701		M3958		M3959+MOD. 701		M39AA+RT21		M39AB+RT21		M39AC+RT21	
Cycles	Hrs.	Weight Change %	Remark	Weight Change %	Remark	Weight Change %	Remark	Weight Change %	Remark	Weight Change %	Remark	Weight Change %	Remark
173	18.5	.032		.015		.028		.044		.045		.044	
378	40	.028		.027		.048		.076		.075		.030	
472	50	.024		.027		.052		.081		.084		.025	
585	62	.023		.028		.050		.018	Fail Pt. Spall	.080	Fail Pt. Spall	.008	Fail Point
755	80	.021		.030		.048		-.18		.063	Spall .1cm^2	.12	
945	100	.018		.022		.045				-.014			
1135	120	-.015	Failure Point	-.014	Failure Point	.044							
1325	140	-.110		-.034		.028							
1510	160					.015							
1700	180					.012							
1890	200					-.02	Failure Point						
Failed At		120 Hrs.		120 Hrs.		200 Hrs.		62 Hrs.		62 Hrs.		70 Hrs.	
C. L. [b]		90		104		137		52		58		66	

a: See Table 2 for Coating Data.

b: C. L. = Coating Life in Minutes/Micron of Coating Thickness.

OXIDATION/CORROSION TEST DATA

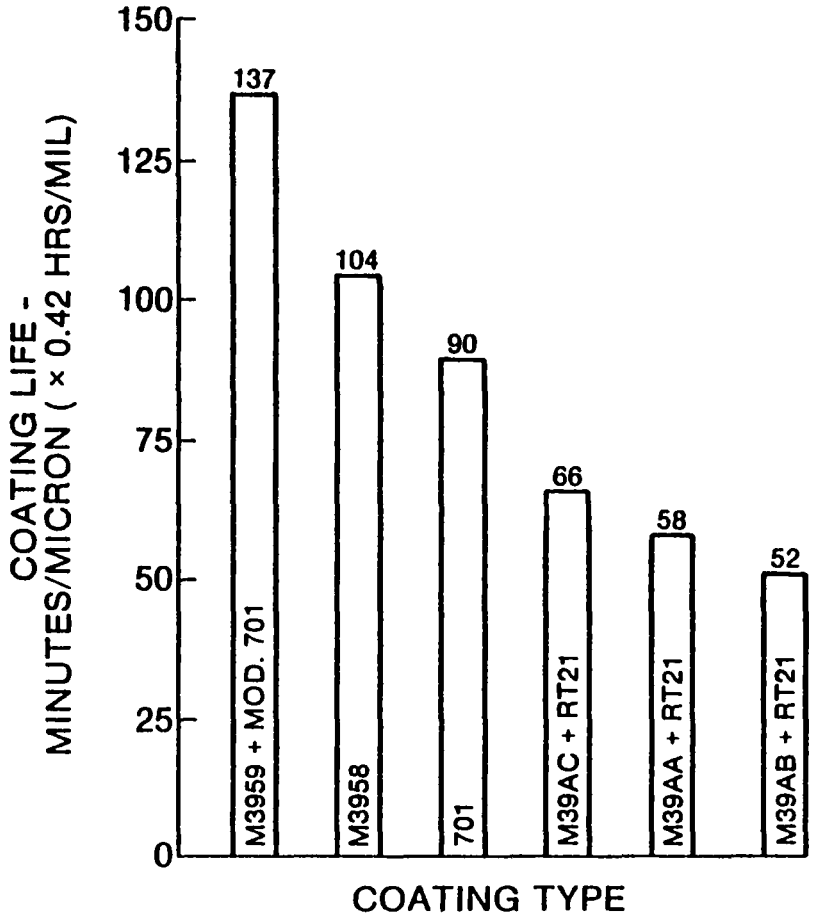

Figure 35 Relative Performance of Various Coatings in Oxidation/Corrosion Based on Normalized Coating Life.

M3958 (12% Al-NiCoCrAlY) and 701 aluminide by a factor of 1.3 and 1.5 respectively. Figure 36 compares the surface appearance of the 701, M3958 and M3959 + Mod. 701 test paddles after 140 hours (1325 cycles) of testing. Both the 701 and M3958 coating had failed at this juncture, while the M3959 + Mod. 701 system underwent further testing.

The M39AC + RT21 exhibited similar coating degration as the baseline 701 aluminide. Figure 37 shows the appearance of this coating after 62 hours of testing (585 cycles). Figure 38 illustrates the reason for termination of the oxidation/corrosion testing for the M39AC + RT21 coating system. Though the coated layer was retained on the curved surfaces of the test paddle, the base metal was exposed along the trailing edge radius due to complete spallation of the NiCoCrY (M39AC) and consequently of the RT21 aluminide. Improper spray parameters and or processing of the M39AC undercoat, particularly near the critical trailing edge radius could have resulted in the total spallation of the undercoat and the overcoat. This also accounts for the drop in weight changes (see Table 5) during the oxidation/corrosion test.

Coating failure by spallation was observed in the M39AA + RT21 (Figure 39) and M39AB + RT21 (Figure 40) systems. The M3959 + Mod. 701 coating exhibited a life 200% greater than NiCoCrY + RT21 systems (Figure 35). The comparative low life of the M39AA + RT21 and M39AB + RT21 coating systems is attributed to the spalling of the aluminum-rich outer layer due to porosity formation along the interface with the undercoat. The highest coating life for the M3959 + Mod. 701 coating system could be due to (1) lower spalling tendency of the aluminum-rich outer layer possibly due to a graded coating with the plasma sprayed undercoat, (2) general overall level of aluminum content and (3) back up of an oxidation/corrosion resistant (6% Al-CoNiCrAlY) undercoat.

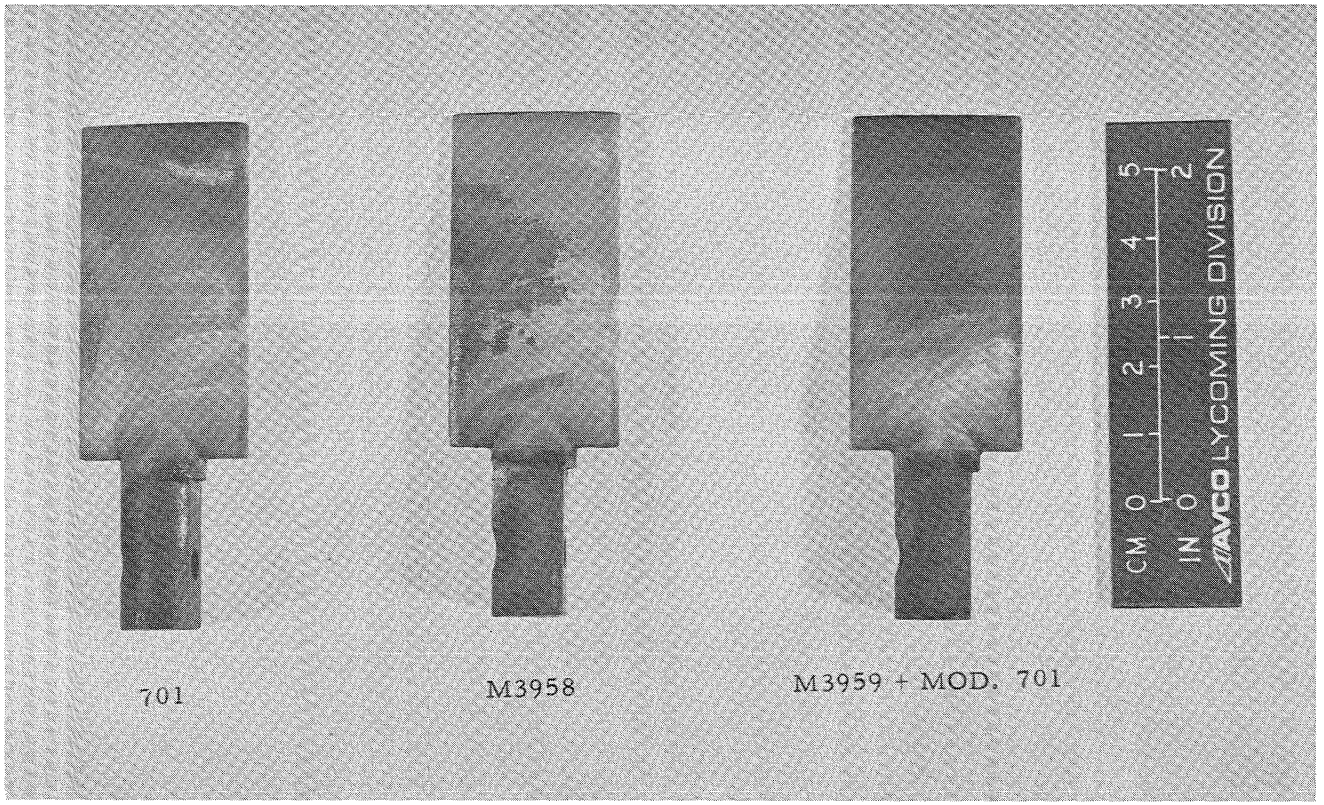

Figure 36 Appearance of 701, M3958 and M3959 + MOD. 701 Coated Specimens after 140 Hrs (1325 Cycles) of Oxidation/Corrosion Test.

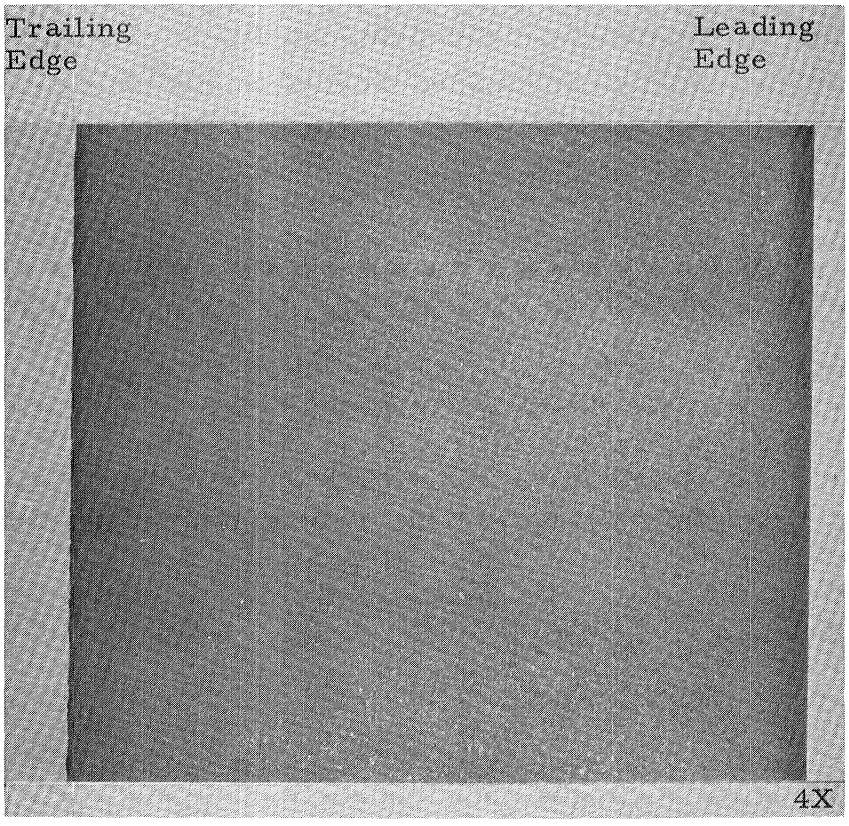

Figure 37 Convex Surface Appearance of M39AC + RT21 Coated Paddle after 62 Hours (585 Cycles) of Oxidation/Corrosion Test.

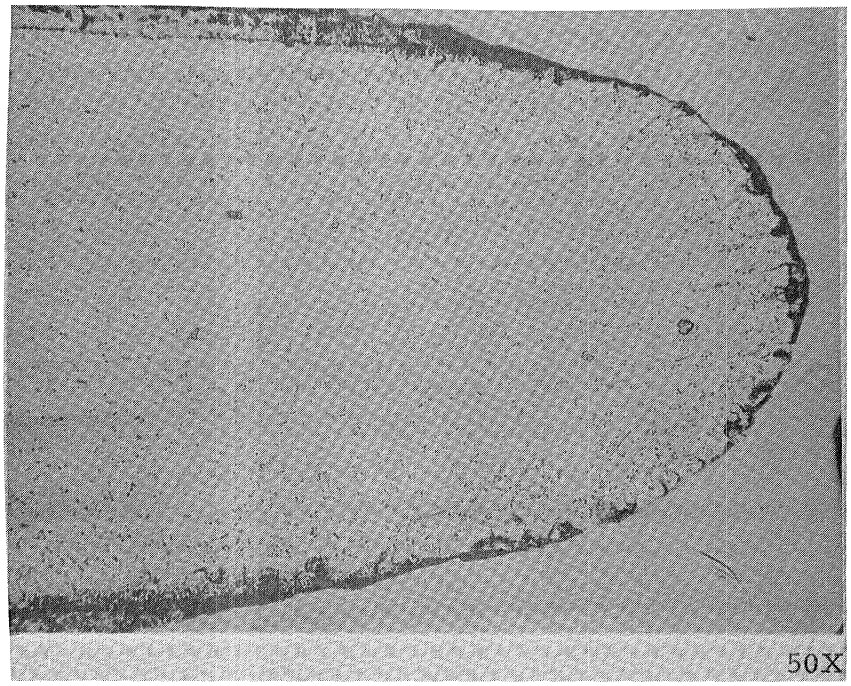

Figure 38 Microstructure showing Spalled Coating on Trailing Edge Radius of M39AC + RT21 Coated Specimen after 80 Hours (755 Cycles) of Oxidation/Corrosion Test.

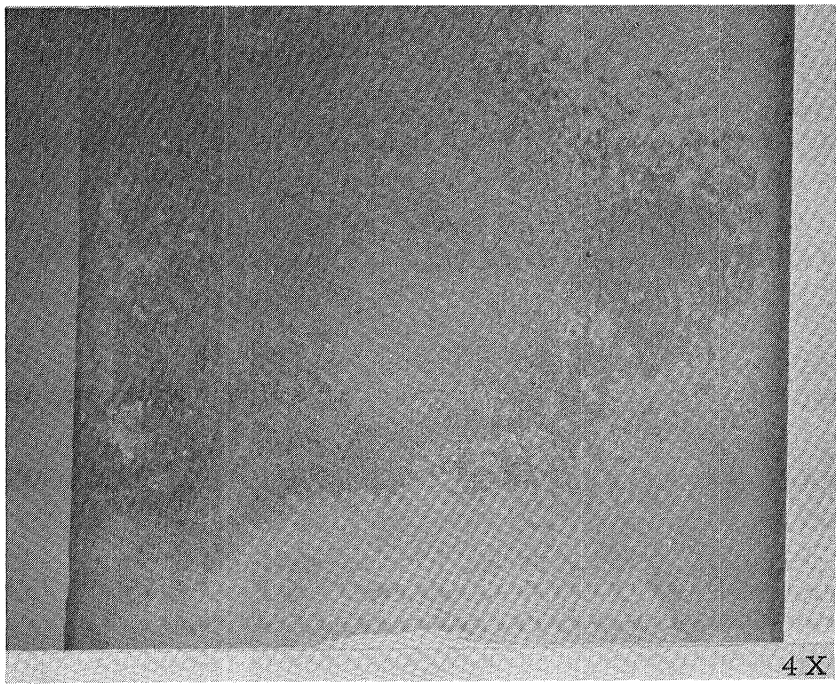

Figure 39 Convex Surface Appearance of M39AA + RT21 Coated Test Paddle after 62 Hrs (585 Cycles) of Oxidation/Corrosion Test. Coating Failure by Spallation Near Trailing Edge.

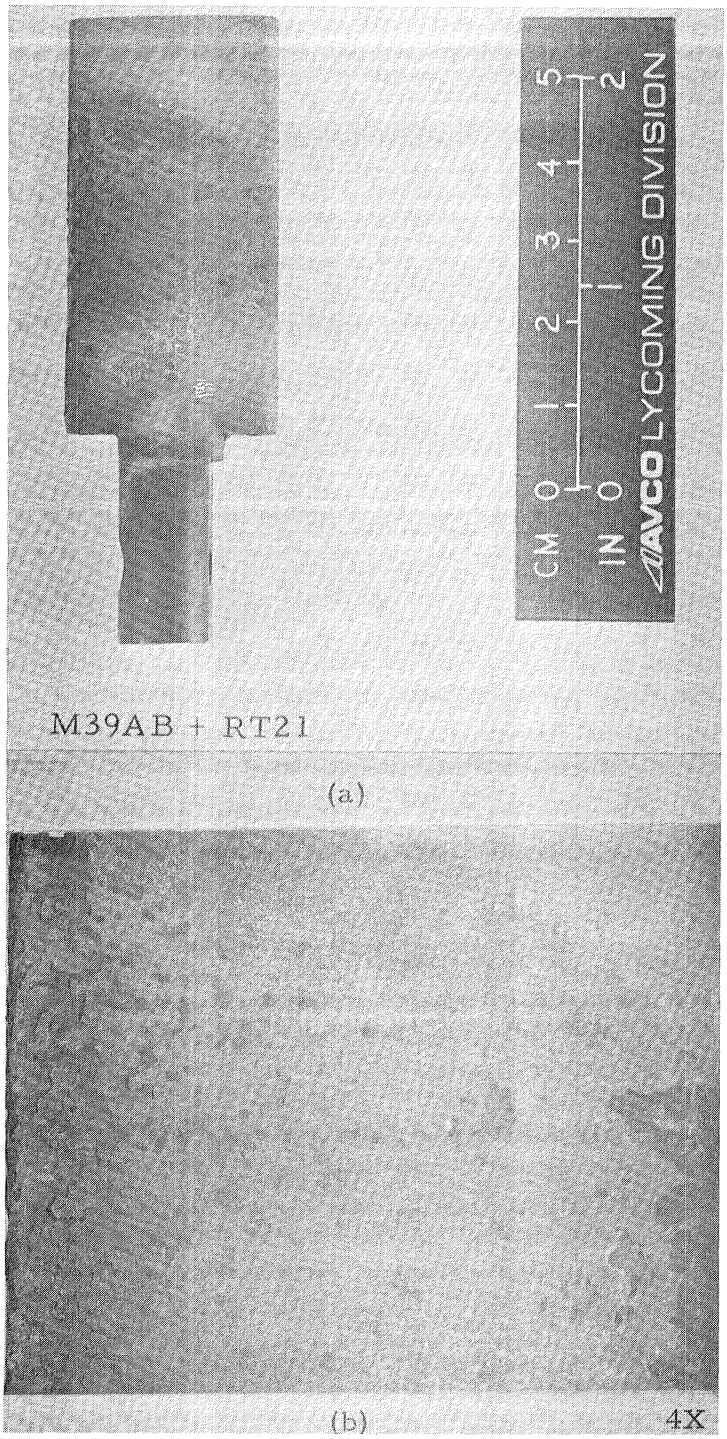

Figure 40 a) Appearance of M39AB + RT21 Coated Test Paddle After 100 Hours (945 Cycles) of Oxidation/Corrosion Test. b) Close Up of Convex Surface of above Paddle. Coating Failure by Spallation.

4.3.1 Metallurgical Evaluation

The metallurgical evaluation was primarily conducted to ascertain the changes in microstructures of the coating systems and identify the principal mode of coating degradation. The elemental probe profile near a failed region of M3959 + Mod. 701 coating is shown in Figure 41. A microstructure has also been included for reference. The coating degradation is due to the gradual depletion of the outer aluminum rich layer through oxidation (compare Figure 41 with the as coated system in Figure 16). A possible reason for the superior performance of the M3959 + Mod. 701 system when compared to the 701 coating (see Figures 11 and 41) could be the presence of cobalt and chromium in the aluminum-rich layer of the former system which could enhance its oxidation/corrosion resistance. Figure 42 shows the microstructure of the failed region of the M3959 + Mod. 701 and the X-ray image photographs indicate the distribution of elements after 200 hours (1890 cycles) of oxidation/corrosion test. The X-ray image for Cr shows that it tends to be the protective oxide during the later stages of oxidation.

The microstructure of a failed region and the corresponding X-ray image elemental distributions of a M3958 (12% Al-NiCoCrAlY) coating after 140 hours (1325 cycles) of testing is shown in Figure 43. The coating degradation was primarily due to oxidation combined with a mild corrosion/sulfidation type pitting attack [greyish area representing Cr (S, O)]. Figure 44 represents a failed area of the 701 coating after 140 hours (1325 cycles) of test. Figure 45 represents the microstructural features and the X-ray element image photographs near a failed region of the 701 coating. The 701 coating failed by the gradual loss of aluminum content through oxidation combined with a mild corrosive attack (dark areas) through the coating.

Figure 46 represents the microstructure and microprobe profile of

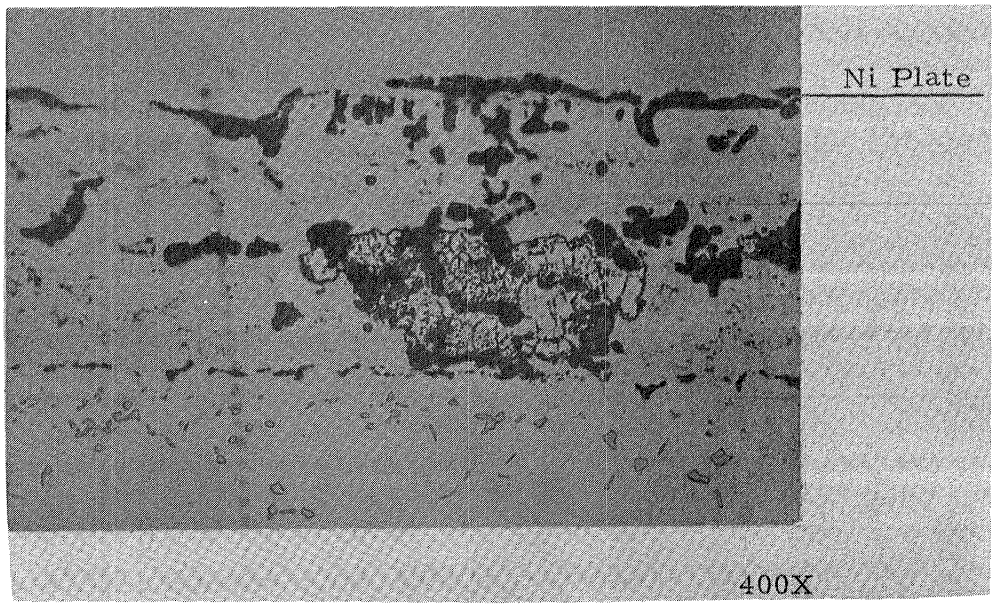

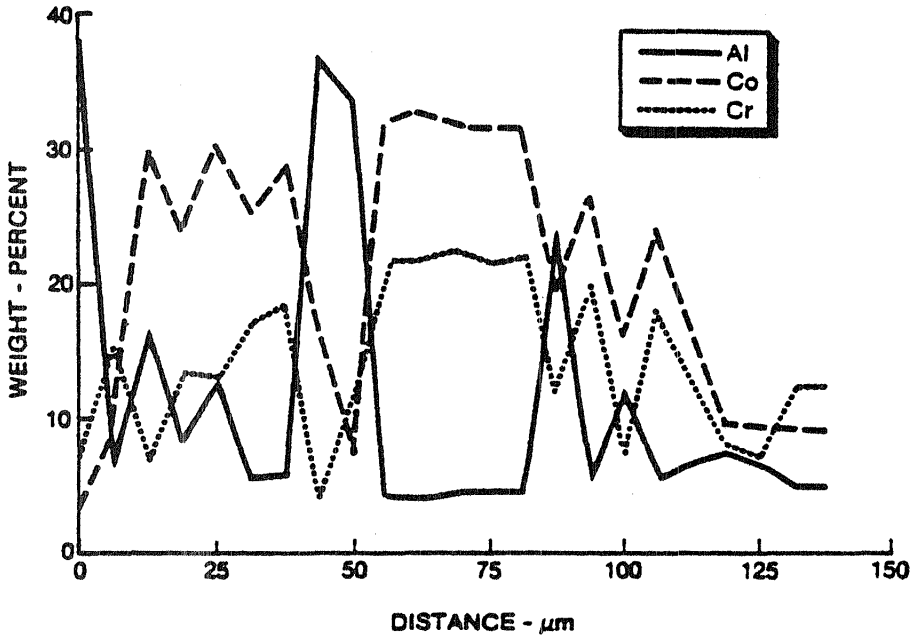

Figure 41 Microstructure and Microprobe Profile Near Failed Region of M3959 + Mod. 701 Coated Specimen After 200 Hours (1890 Cycles) of Oxidation/Corrosion Test.

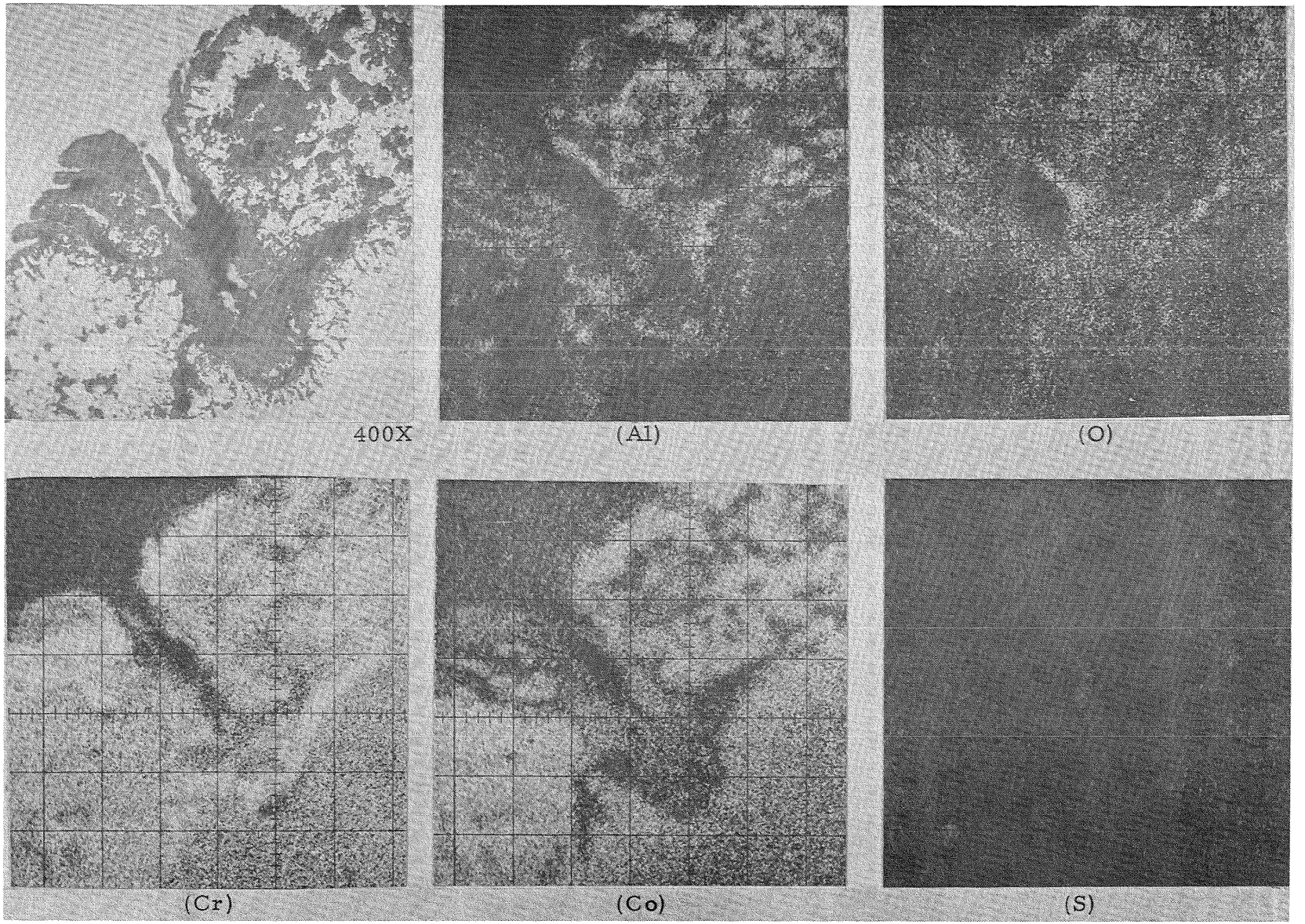

Figure 42 X-Ray Images Showing Distribution of Al, O, Cr, Co, S in Failed Region of M3959 + MOD. 701 Coated Specimen after 200 Hours (1890 Cycles) of Oxidation/Corrosion Test.

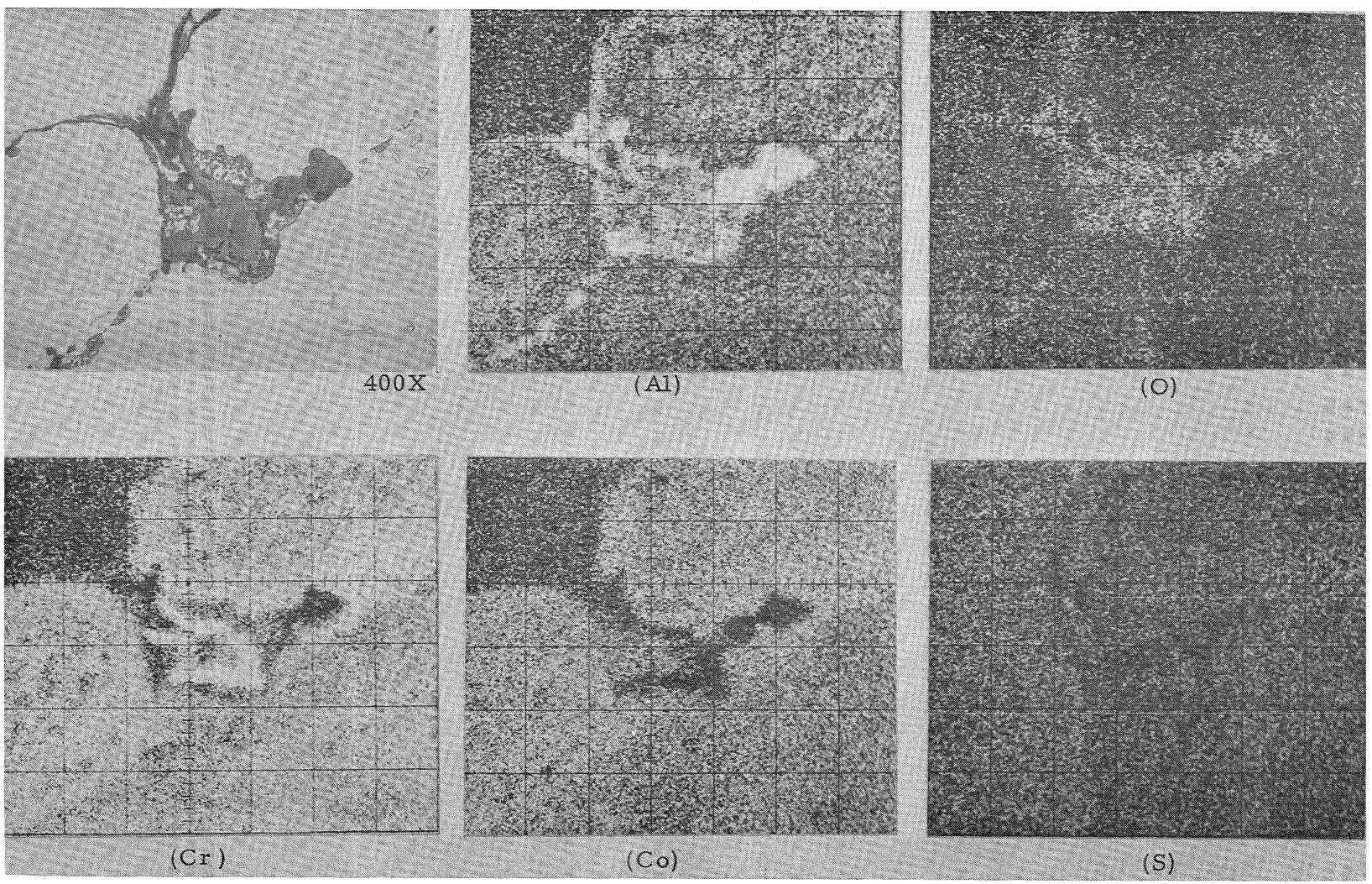

Figure 43 X-Ray Images Showing Distribution of Al, O, Cr, Co, S in Failed Region of M3958 Coated Specimen after 140 Hours (1325 Cycles) of Oxidation/Corrosion Test.

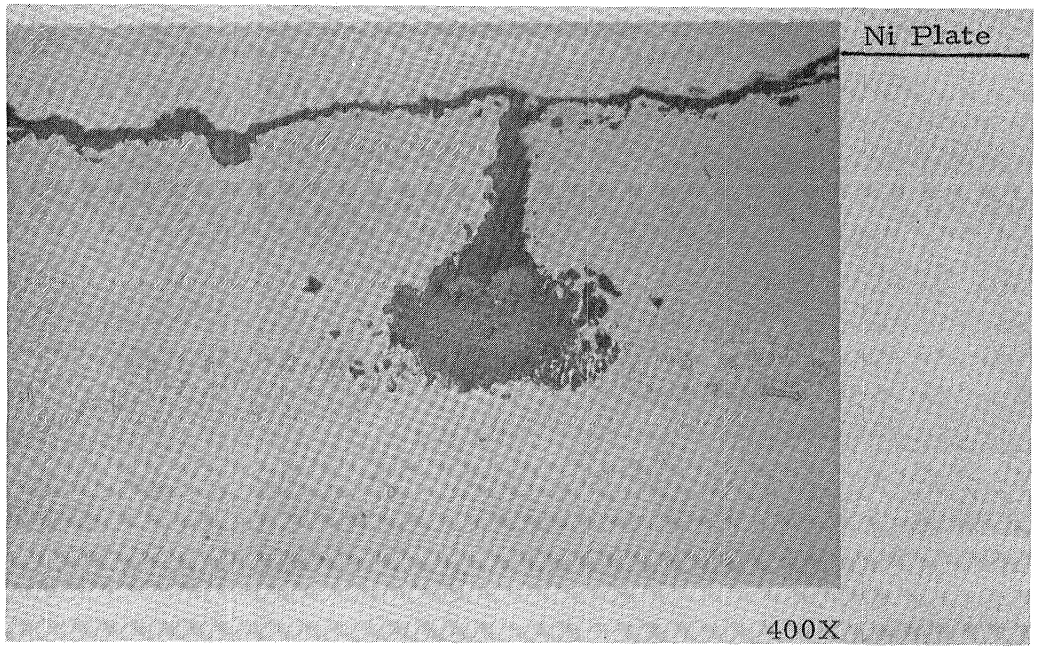

Figure 44 Microstructure at Failed Section of 701 Coating after 140 Hours (1325 Cycles) of Oxidation/Corrosion Test.

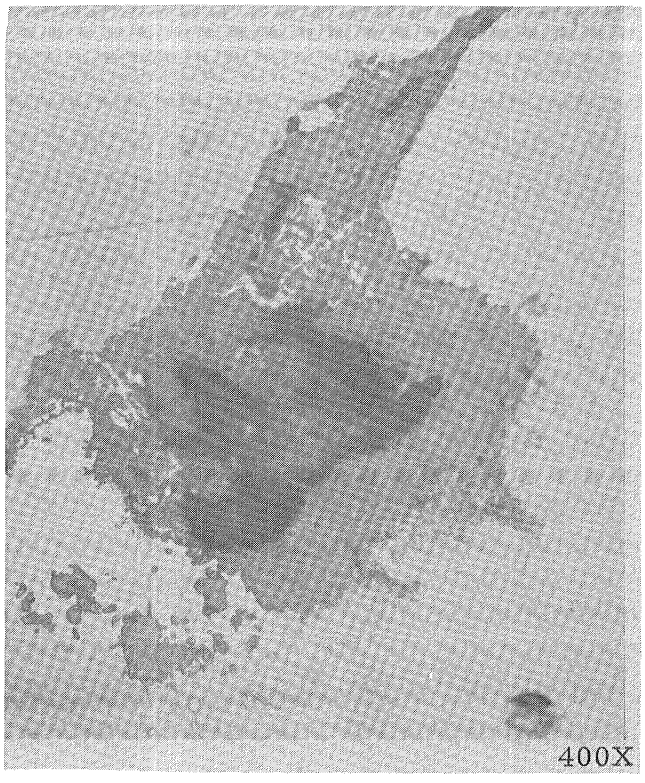

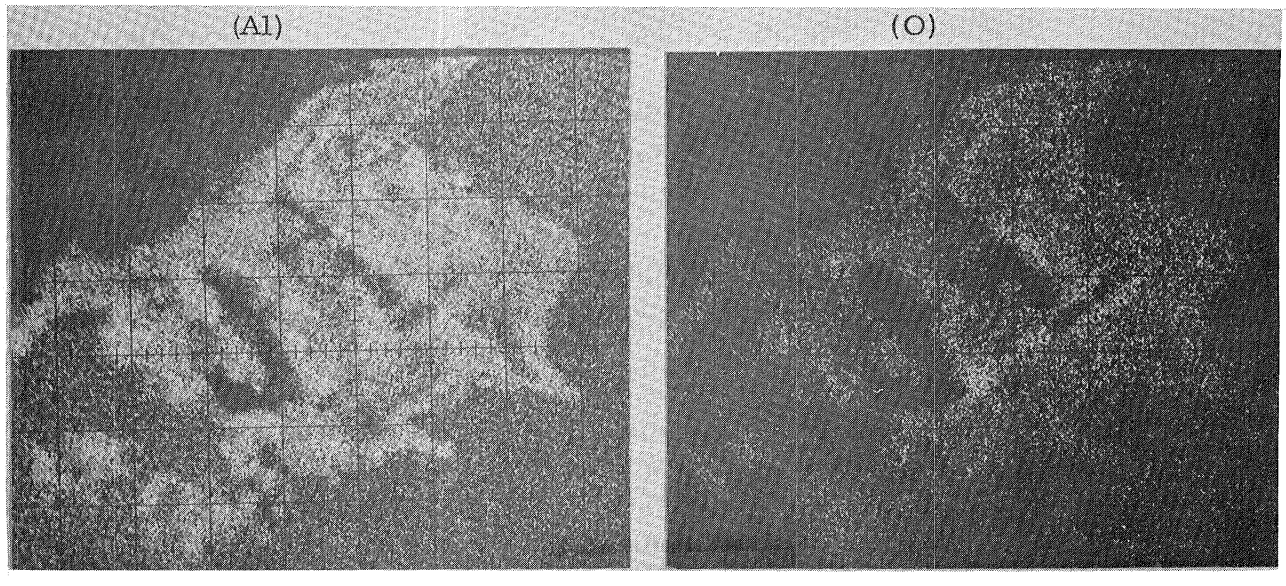

Figure 45 X-Ray Images Showing Distribution of Al, O in Failed Section of 701 Coating after 140 Hours (1325 Cycles) of Oxidation/ Corrosion Test. (Figure 45 cont'd on next page).

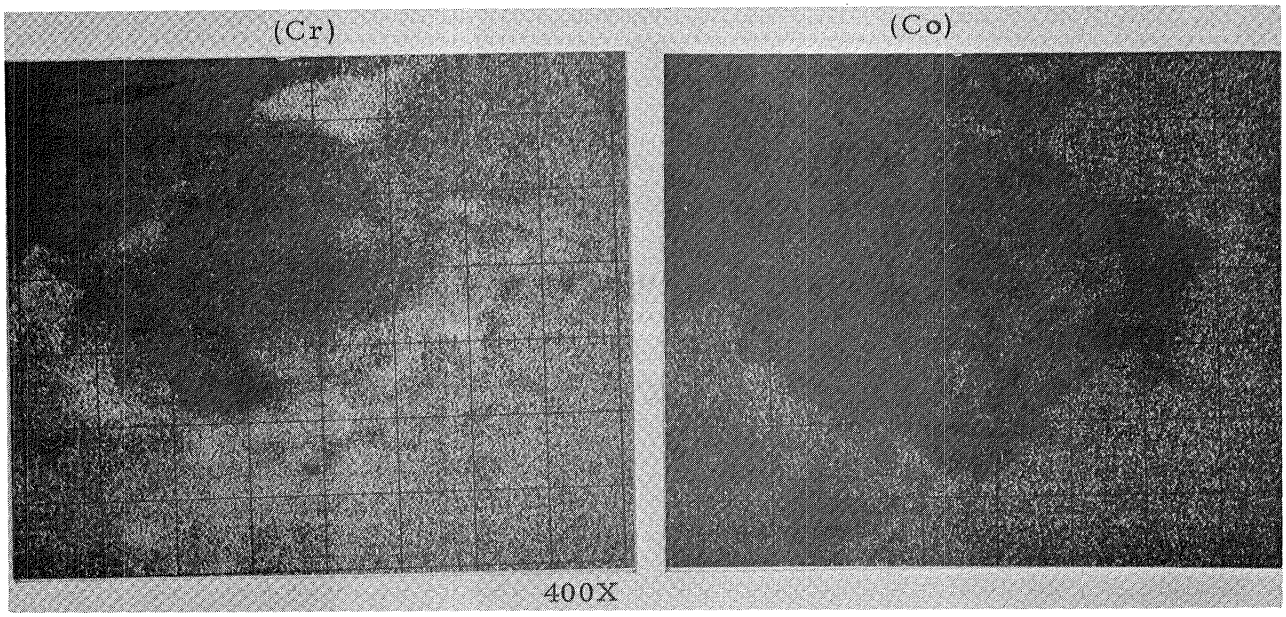

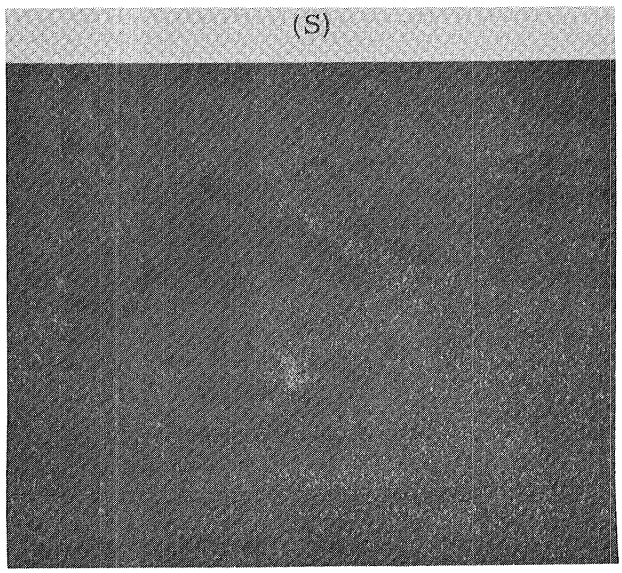

Figure 45(cont'd) X-Ray Images Showing Distribution of Cr, Co, S in Failed Section of 701 Coating after 140 Hours (1325 Cycles) of Oxidation/Corrosion Test.

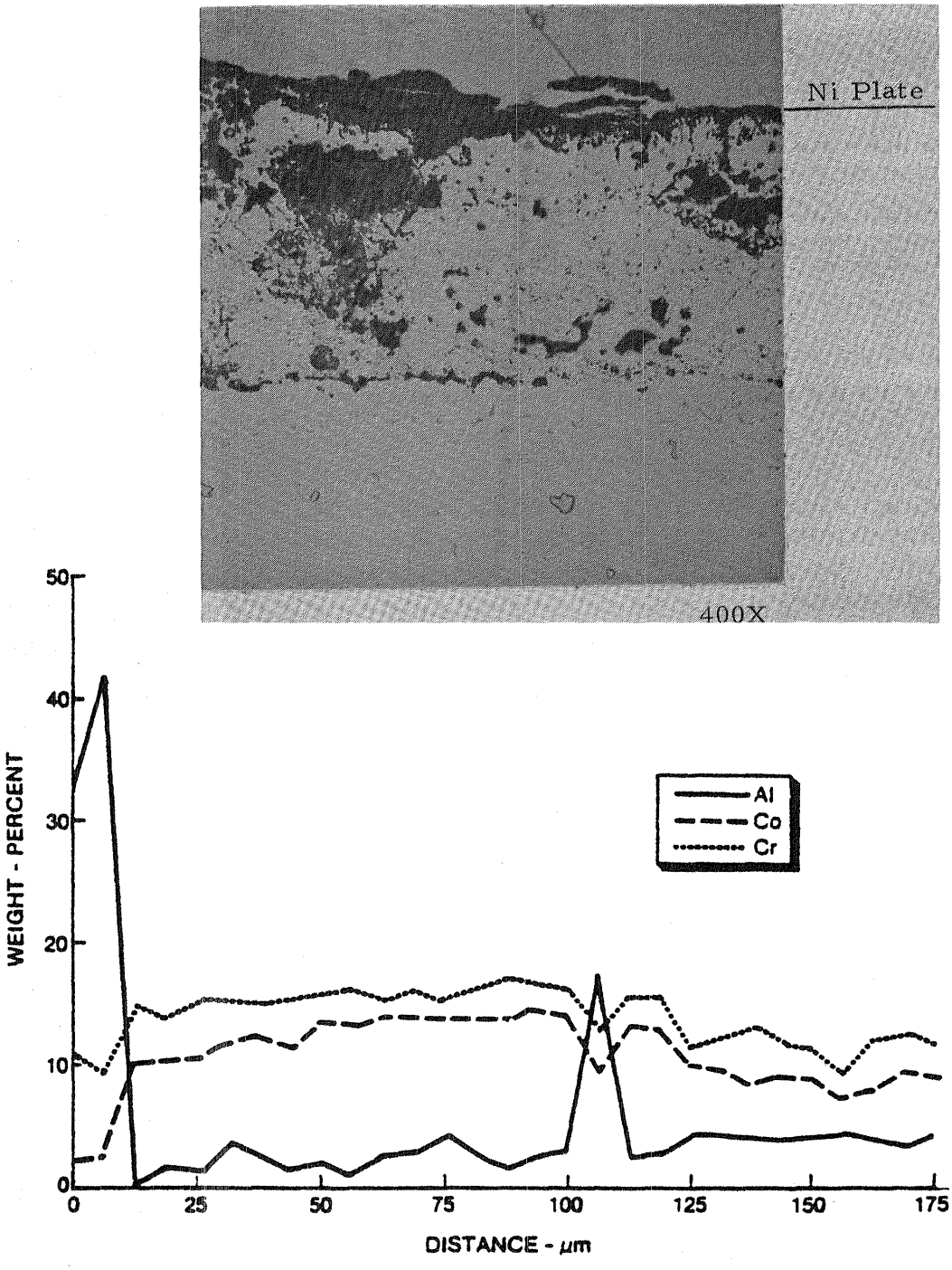

Figure 46 Microstructure and Microprobe Profile of M39AC + RT21 Coated Specimen After 80 Hours (755 Cycles) of Oxidation/Corrosion Test.

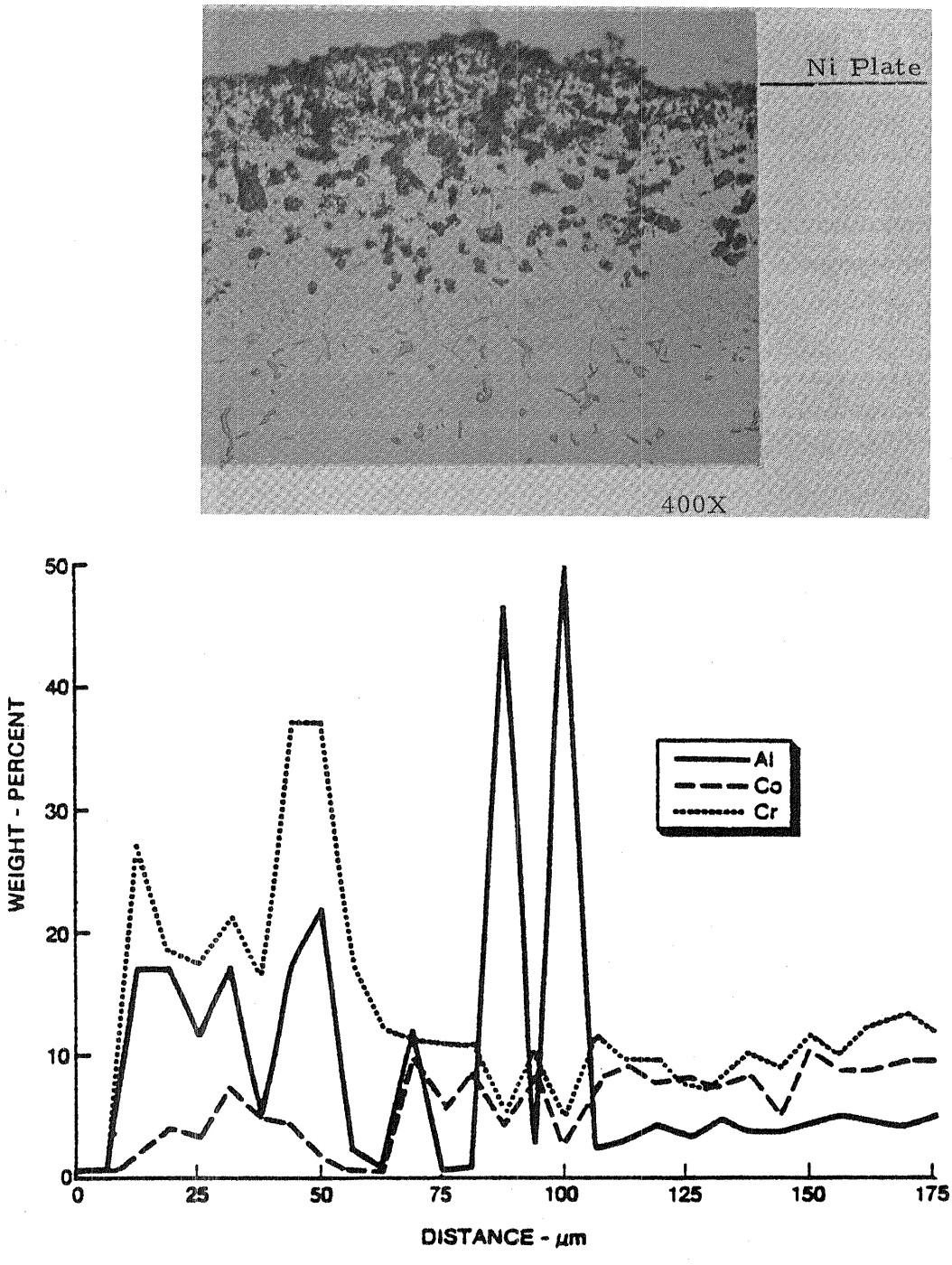

Figure 47 Microstructure and Microprobe Profile Near Failed Region of M39AA + RT21 Coated Specimen After 80 Hours (755 Cycles) of Oxidation/Corrosion Test.

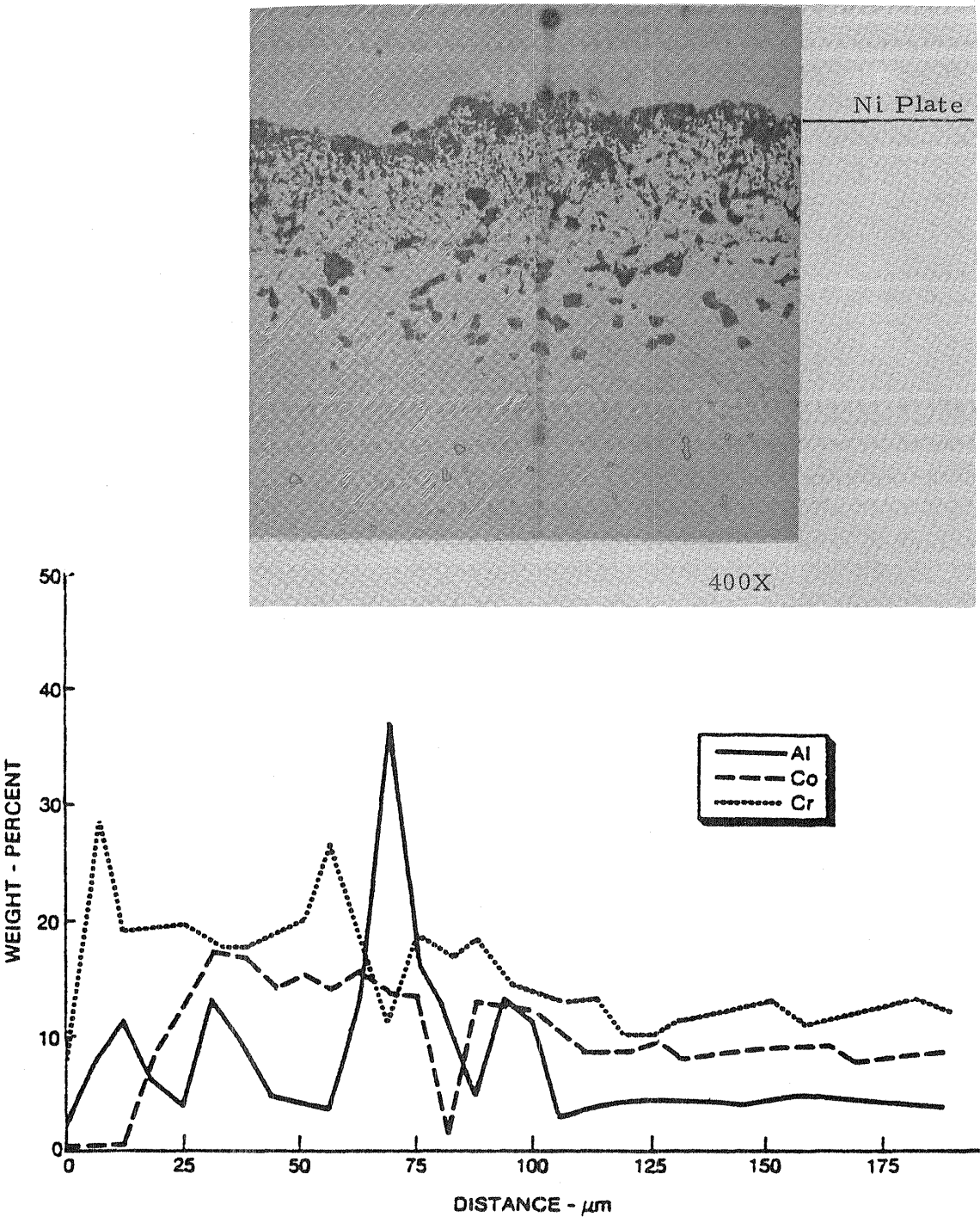

Figure 48 Microstructure and Microprobe Profile Near Failed Region of M39AB + RT21 Coated Specimen After 100 Hours (945 Cycles) of Oxidation/Corrosion Test.

M39AC + RT21 coated specimen after 80 hours (755 cycles) of test. The coating degradation mechanism was similar to the baseline 701 aluminide coating. Figures 47 and 48 represents the post-test microstructures and the elemental microprobe profiles near a failed region for the M39AA + RT21 and M39AB + RT21 coating systems. Both systems showed similar characteristics in failure in that the outer aluminum rich layer had spalled (compare Figures 47 and 48 with the as-coated systems in Figures 17 and 18) and that chromium had taken over as the protective oxide. As mentioned before, this spallation/separation effect of the outer aluminum-rich layer is generally attributed to the high Cr content (35 w/o) and absence of Al in the plasma sprayed M39AA and M39AB undercoat compostion.

5.0 CONCLUSIONS

The metallurgical evaluation, thermal fatigue and oxidation/corrosion data for the 10 coating systems which included six candidate two-step coatings [(NiCoCrY, CoNiCrAlY) + aluminide] necessary for proper coverage of all surfaces of an integral or segmented nozzle indicate the following conclusions:

(1) The plasma sprayed 12% Al-NiCoCrAlY (M3958) coating exhibited the best performance in thermal fatigue resistance amongst the 10 coating systems tested. However a single-step plasma spray coating cannot effectively cover all surfaces of an integral or segmented nozzle.

(2) Thermal fatigue tests indicated that the Group I (M3958) coating out performed Group II (701, Mod. 701, M3959 + 701 and M3959 + Mod. 701), Group III (M39AC + RT21 and M39AC + Mod. 701) and Group IV (RT21, M39AA + RT21 and M39AB + RT21) coatings by a factor of 1.5, 1.88 and 2.5 respectively in cycles to crack initiation.

(3) Thermal fatigue tests of the various aluminide systems indicated that NiAl exhibited similar thermal cracking characteristics for an aluminum content between 25 w/o - 40 w/o. The 701 aluminides (32 - 40 w/o Al) tested were hyperstoichiometric in nature.

(4) All fatigue cracks which propogated through the substrate were intergranular in nature. For the duplex systems which involved a plasma sprayed undercoat and aluminide overcoat, the crack initiated in the outer high aluminum content layer with progressive propogation through the undercoat and finally into the substrate.

(5) The high Cr (35 w/o) - NiCoCrY + Aluminide systems (non-graded aluminum content coating structure) indicated a generalized fatigue failure mode of cracking in the aluminide combined with a separation of the outer high-aluminum content layer from the NiCoCrY underlayer.

(6) Oxidation/corrosion test data indicated that the 6% Al-CoNiCrAlY (M3959) + Mod. 701 coating system had the longest coating life amongst the 6 coating systems tested. This coating, along with the 701 aluminides, was in the group of coatings rated second best in thermal fatigue. The plasma sprayed 12% Al-NiCoCrAlY (M3958) was rated the best in thermal fatigue and ranked second in oxidation/corrosion, with its life in the latter test significantly better than the aluminides. However, as mentioned before, this coating is not applicable to integral nozzles.

(7) The coating life of M3959 + Mod. 701 in oxidation/corrosion was greater than M3958, 701 and the NiCoCrY + RT21 systems by a factor of 1.3, 1.5 and 2 respectively.

(8) The presence of low Al ($\sim$ 6 w/o) in the plasma sprayed undercoat facilitates the formation of a graded aluminum content coating on pack aluminizing.

(9) Excessive Cr content ($\sim$ 35 w/o) in the plasma (NiCoCrY) sprayed undercoat leads to the formation of a Cr-rich layer at the plasma spray-aluminide interface on pack aluminizing. This layer acts as a diffusion inhibitor for aluminum and makes it more difficult to form a graded coating between the outer aluminide and the NiCoCrY undercoat.

A graded aluminum content coating in the NiCoCrY + aluminide systems can be obtained by lowering the chromium content in the plasma spray undercoat and modifying the pack process by the use of an "inward diffusion" aluminide overcoat.

6.0 RECOMMENDATION

The trend for future development work of advanced two-step [(NiCoCrY, NiCoCrAlY) + aluminide] coating systems, applicable for integral or segmented nozzles, should be directed towards a lower chromium content plasma spray composition to inhibit the Cr-rich layer formation at the plasma spray-aluminide interface after aluminizing. Likewise the objective of achieving a graded aluminum content in the plasma sprayed underlayer can be obtained by the use of 1) a low aluminum content underlayer or 2) a NiCoCrY underlayer combined with an "inward diffusion" aluminide overcoat.

REFERENCES

1. Goward G. W., J. Metals, Vol. 22, pg. 31 (1970)
2. Hecht R., Goward G., and Elam R., "High Temperature NiCoCrAlY Coatings", US Patent 3, 928, 026 (1975)
3. Goward G. W., Boone D. H., and Pettit, F. S., "High Temperature Oxidation Resistant Coating Alloy", US Patent 3, 754, 903. (1973)
4. Gedwill, M. A., and Grisaffe, S. J., "Duplex Aluminized Coatings", US Patent 3, 869, 779 (1975)
5. Gedwill, M. A., and Grisaffe S. J., Oxidation Resistant Claddings for Superalloys, NASA TMX-67925, 1971
6. Bizon, P., Private Communication.

APPENDIX - A

THERMAL FATIGUE DATA

APPENDIX - A

Table A - 1

Thermal Fatigue Performance of Coated Wedge Bars. Fast Quench Rate. Data on Small Radius (R = 0.635 mm)

Cycles[1]	Individual Crack Length, mm[2] 1st Crack (A)	2nd Crack (B)	3rd Crack (C)	Calculated Avg. Crack Length, mm $\frac{A+B+C}{3}$	Total Cracks Observed
		701 (Specimen No. A36)			
400	No Crack	No Crack	No Crack		
500	0.635	"	0.20	0.28	2
650	2.54	1.27	0.76	1.52	4
800	3.3	2.03	1.27	2.20	5
		RT21 (Specimen No. A8)			
300	Craze Cracks	Craze Cracks	Craze Cracks		cc.
400	"	"	"		"
500	1.14	1.01	0.89	1.01	4, cc.
650	4.06	3.04	2.03	3.04	6, " .
		M3958 (Specimen No. A12)			
500	No Crack	No Crack	No Crack		
650	2.28	0.76	"	1.01	2
		M39AA+RT21 (Specimen No. A31)			
300	Craze Cracks	Craze Cracks	Craze Cracks		cc.
400	"	C.S.C.	C.S.C.		csc
650	4.06	2.15	0.25	2.15	15, s
900	6.09	2.79	0.51	3.13	18, s
		M39AA+RT21 (Specimen No. A34)			
300	Craze Cracks	Craze Cracks	Craze Cracks		cc.
400	"	"	"		csc.
650	"	"	"		"
800	4.19	2.16	1.01	2.45	18, cc,s
900	7.87	2.79	1.27	4.31	23, cc,s

cc = crazing cracks, csc = closely spaced cracks, e = eruption, s = spall, mc = mild cracks.

1. Test cycle - See Fig. 7.
2. Crack length - average of measurements from both sides.

TABLE A - 1 (Cont'd)

Cycles[1]	Individual Crack Length, mm 1st Crack (A)	2nd Crack (B)	3rd Crack (C)	Calculated Avg. Crack Length, mm. $\frac{A+B+C}{3}$	Total Cracks Observed
		M39AB+RT21 (Specimen No. A30)			
300	Craze Cracks	Craze Cracks	Craze Cracks		cc.
400	"	"	"		"
500	1.52	.38	No Crack	0.63	2, cc.
650	2.79	1.01	(see last column)	1.26	22, cc, e
900	3.81	1.27	1.27	2.11	30, e, s
		M39AB+RT21 (Specimen No. A28)			
300	Craze Cracks	Craze Cracks	Craze Cracks		cc.
400	"	"	"		"
500	.96	.96	.96	0.96	15, csc
650	1.27	1.27	1.27	1.27	25, cc, e
900	3.175	1.58	1.27	2.00	27, e, s
		M39AC+RT21 (Specimen No. A19)			
300	No Crack	No Crack	No Crack		
400	C.C.	C.C.	"		cc.
500	0.25	0.25	No Crack	0.166	2, cc.
650	3.05	1.27	"	1.44	2, mc.
800	4.06	2.79	(see last column)	2.28	2, 6mc.
900	4.44	3.17	"	2.53	2, 10mc.
		M39AC+RT21 (Specimen No. A27)			
300	No Crack	No Crack	No Crack		
400	C.C.				cc.
500	0.51	0.25	No Crack	0.253	2, cc.
650	2.79	1.27	"	1.35	"
800	4.31	2.54	"	2.28	"
900	5.58	3.04	"	2.87	"

Table A - 2

Thermal Fatigue Performance of Coated Wedge Bars. Slow Quench Rate. Data on Small Radius (R = 0.635 mm)

Cycles[1]	Individual Crack Length, mm[2] 1st Crack (A)	2nd Crack (B)	3rd Crack (C)	Calculated Avg. Crack Length, mm $\frac{A+B+C}{3}$	Total Cracks Observed
		701 (Specimen No. A38)			
600	No Crack	No Crack	No Crack		
750	0.38	"	"	0.12	1
900	1.27	"	"	0.42	1
1 050	2.16	"	"	0.72	1
1 200	4.70	0.50	0.50	1.9	3
1 350	5.08	1.27	0.50	2.28	4, cc.
1 500	5.46	2.16	0.50	2.70	4, "
1 650	5.72	2.41	0.50	2.88	5, "
1 800	6.00	2.46	0.50	2.99	5, "
1 950	6.98	2.54	0.63	3.38	6, "
2 100	7.24	2.92	0.70	3.62	7, "
2 250	7.62	3.05	0.76	3.81	7, "
		MOD. 701 (Specimen No A39)			
600	No Crack	No Crack	No Crack		
750	"	0.50	0.50	0.33	2
900	"	0.76	0.76	0.50	2
1 050	5.08	0.89	1.01	2.32	3
1 200	6.35	1.40	1.14	2.96	3
1 350	6.85	1.52	1.27	3.21	4, cc.
1500	7.11	1.77	1.39	3.42	5, cc.
		MOD. 701 (Specimen No. A41)			
600	No Crack	No Crack	No Crack		
750	0.89	"	"	0.296	1

cc = crazing cracks, e = eruptions, s = spall, csc = closely spaced cracks

1. Test cycle - See Figure 7
2. Crack length - average of measurements from both sides.

Table A - 2 (Cont'd)

Cycles[1]	Individual Crack Length, mm[2] 1st Crack (A)	2nd Crack (B)	3rd Crack (C)	Calculated Avg. Crack Length, mm $\frac{A+B+C}{3}$	Total Cracks Observed
900	3.93	No Crack	No Crack	1.31	1
1050	4.57	"	"	1.52	1
		RT21 (Specimen No. A10)			
300	No Crack	No Crack	No Crack		
450	1.65	"	"	0.55	1, cc.
600	3.81	1.14	0.51	1.82	9,"
750	4.31	1.77	0.89	2.32	13,"
900	4.82	2.54	1.01	2.87	16,"
1050	5.58	2.92	1.27	3.38	16,"
		M3958 (Specimen No. A7)			
900	No Crack	No Crack	No Crack		
1050	4.70	"	"	1.56	1
1200	5.08	"	"	1.69	1
1350	5.58	"	"	1.86	1
1500	6.10	0.51	"	2.20	2
		M3959+701 (Specimen No. A3)			
450	No Crack	No Crack	No Crack		
600	"	0.89	"	0.3	1
750	"	1.40	0.51	0.63	2
900	"	1.52	0.76	0.76	2
1050	5.08	1.90	1.01	2.66	3, e
1200	5.84	2.03	1.14	3.00	14
1350	6.47	2.29	1.52	3.42	18
1500	6.73	2.54	2.03	3.76	22, e
		M3959+701 (Specimen No. A9)			
600	No Crack	No Crack	No Crack		

Table A - 2 (Cont'd)

Cycles[1]	Individual Crack Length, mm[2] 1st Crack (A)	2nd Crack (B)	3rd Crack (C)	Calculated Avg. Crack Length, mm $\frac{A+B+C}{3}$	Total Cracks Observed
750	C.S.C.	C.S.C.	C.S.C.		5, e, s
900	2.79	"	"	0.93	8
1050	4.44	"	"	1.48	18
	M3959+MOD. 701 (Specimen No. A13)				
600	No Crack	No Crack	No Crack		
750	3.30	"	"	1.1	1
900	5.33	"	"	1.77	1
1050	5.84	"	"	1.94	1
1200	6.22	3.175	-	3.13	2, cc.
1350	6.73	4.06	-	3.59	"
1500	6.98	4.31	-	3.76	"
	M3959+MOD. 701 (Specimen No. A5)				
450	No Crack	No Crack	No Crack		
600	1.27	"	"	0.42	1
750	3.17	1.14	"	1.44	2
900	3.55	1.52	"	1.69	2, cc.
1050	3.81	2.03	"	1.95	2, cc.
	M39AC+MOD. 701 (Specimen No. A23)				
450	No Crack	No Crack	No Crack		
600	4.06	"	"	1.35	1
750	4.57	"	"	1.52	1
900	5.08	"	"	1.69	1
1050	5.33	"	"	1.77	1, cc.
1200	5.58	"	"	1.86	1, "
1350	5.84	1.65	"	2.49	1, "
1500	6.09	3.55	0.76	3.46	3, "

Table A - 2 (Cont'd)

Cycles[1]	Individual Crack Length[2], mm: 1st Crack (A)	2nd Crack (B)	3rd Crack (C)	Calculated Avg. Crack Length, mm $\frac{A+B+C}{3}$	Total Cracks Observed
		M39AC+MOD. 701 (Specimen No. A25)			
450	No Crack	No Crack	No Crack		
600	cc.	cc.	cc.		cc.
750	2.03	0.38	0.38	0.93	3, cc.
900	2.54	1.01	0.76	1.43	3, cc.
1050	2.92	1.52	1.01	1.81	3, cc.

End of Document